THE FERMILAB BOOSTER RF MODIFICATIONS FOR THE 800MEV INJECTION ERA

Victor M. Grzelak

Submitted to the faculty of the University Graduate School in partial fulfillment of the requirements for the degree

Master of Science

in the Department Physics

Indiana University

May 2023

Accepted by the Graduate Faculty, Indiana University, in partial fulfillment of the requirement for the degree of Master of Science.

Master's Thesis Committee

_____

[W. Michael Snow, Ph.D.]

_____

[P. Derwent, Ph.D.]

_____

[R. Tayloe, Ph.D.]

_____

[C. Palatchi, Ph.D.]

Acknowledgements

I would like to thank my wife for her patience and support throughout the entire IU program and the many USPAS classes. Thank you to John Reid for his mentorship and support throughout my career at Fermilab, and for his help in arranging the tests and analysis conducted below. Thank you to Paul Derwent for his support and advice in this thesis process.

I'd like to thank my technical staff and colleagues for helping me carryout the testing. I'd also like to thank Bob Scala, Daren Plant, Efrain Cortez, Matt Domeier, Brian Schupach, Craig Drennan, Gregg Vogel, Mike Kucera, Chandra Bhat, Kent Triplett, Jeff Larson, Salah Chaurize, Matt Slabaugh, Ryan Montiel, and Ken Klotz and C.Y. Tan. I'd also like to thank Susan Winchester and Irina Novitski for their roles with USPAS organization and interfacing with IU.

This document was prepared using the resources of the Fermi National Accelerator Laboratory (Fermilab), a U.S. Department of Energy, Office of Science, HEP User Facility. Fermilab is managed by Fermi Research Alliance, LLC (FRA), acting under Contract No. DE-AC02-07CH11359.

Victor M Grzelak

The Fermilab Booster RF Modifications for the 800MeV Injection Era

Abstract

Fermi National Accelerator Laboratory (FNAL) will be undergoing a large accelerator modification to increase the throughput of particles for high intensity physics (HIP) experiments. The Booster, a rapid cycling synchrotron, will have higher energy at injection, increased machine frequency, and more particles accelerated per cycle. A series of tests were conducted to verify the functionality of the existing RF structures and electronics to operate at this increased rate and intensity. Preliminary results indicate that the Booster cavities will be able to operate in this new regime. Infrastructure modifications will be required for successful operations.

Contents

1. Introduction to Fermilab

Fermi National Accelerator Laboratory, commonly called Fermilab, is home to one of the highest energy proton accelerators in the United States. Colliding high energy protons with various fixed targets allows for the generation of neutrinos, muons, and other elementary particles for physics research. In order to generate the high energy protons for these experiments, a series of particle accelerators is needed.

Every particle accelerator is composed of two primary systems, a containment system, and an acceleration system. Typically a containment system is composed of magnets, which allow for the bending and focusing of charged particle trajectories while minimizing transverse beam emittance. The acceleration system is tasked with providing an energy gain, while minimizing the longitudinal beam emittance. There are three primary proton accelerators in the complex, the Linac (Linear accelerator), the Booster, and the Main Injector.

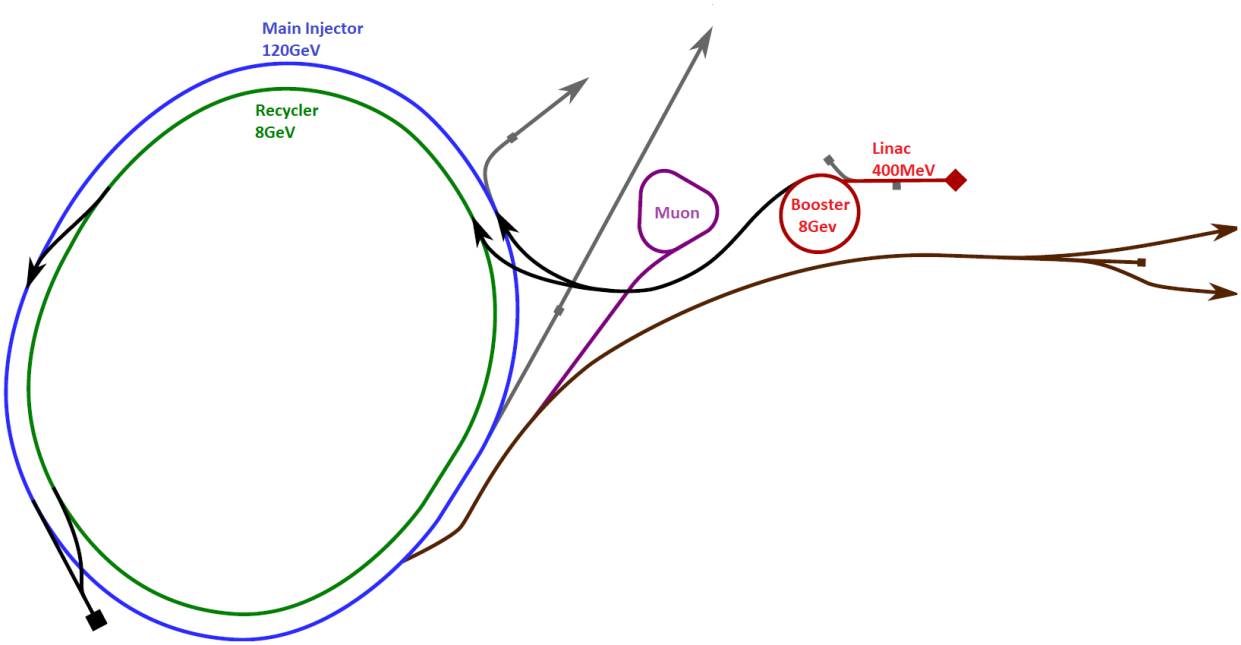

Figure 1-1 Present day Fermilab accelerator complex layout

The following is the path beam takes for the lab's primary experiment for neutrino physics. The RFQ Injection Line (RIL) starts with a magnetron source, which takes hydrogen gas, ionizes it to H-, then begins accelerating the ions electrostatically via a 30kV electric pulse. The next accelerating structure is the Radio Frequency Quadrupole (RFQ) cavity, which uses 201MHz RF fields to bunch and accelerate the beam to 750keV. The output of the RIL is about 5.5e12 H- particles over 50us. [9]

The beam that is extracted from the RIL enters a Linac. The Linac consists of two different accelerating structures: a 201 MHz Drift Tube Linac (DTL), and an 805 MHz Side Coupled Linac (SCL). The DTL is responsible for accelerating the beam from 750keV to 116MeV, and a SCL is responsible for accelerating the beam from 116MeV to 400MeV. [10]

The beam that is extracted from the Linac enters the Booster synchrotron. The beam enters the machine and is stripped of its electrons using graphite stripping foils. The beam begins to circulate, and all the beam is layered via charge exchange injection. During injection there is no acceleration, and the beam undergoes debunching. After the injection period, the beam is re-bunched at a frequency of 37 MHz through an adiabatic process called paraphasing. The synchrotron then accelerates the beam to a kinetic energy of 8GeV. Booster is a rapid cycling synchrotron (RCS), with a machine frequency of 15 Hz. The Booster magnets are part of a large resonant structure, and the ramp is a positive DC offset sinusoid, with beam being injected at the bottom of the sinusoid and extracted near the peak. Booster extracts 5e12 protons every 66ms, this quantity is called a "Booster batch". [7]

The beam extracted from the Booster is injected into the Recycler, which is a non-accelerating synchrotron, utilized for a process called "slip stacking". The recycler only has space for 7 Booster batches, but the RF manipulation known as slip stacking allows for 6 batches to be layered on top of 6 more batches effectively allowing for twelve booster batches. 5.9E13 protons are extracted from Recycler to the Main Injector. [16]

The Main Injector (MI) is the final accelerating synchrotron at Fermilab. The beam is accelerated from 8GeV to 120GeV, over 0.83seconds, the MI machine cycle is 1.4 seconds. About 5.6e13 protons are extracted from the MI and collide with a target generating pions that decay into neutrinos for Fermilab's neutrino experiments. [16]

The primary metric for success of the accelerator complex is the time averaged target beam power, P_{Target}, which is a function of total number of protons, N, kinetic energy, KE, and cycle time, T

$$P_{Target} = \frac{N(KE)}{T} = \frac{5.6e13(120GeV)}{1.4s} = 769kW \quad (1)$$

1.1. Introduction to PIP-II

The Proton Improvement Plan II, PIP-II, is a project that plans to increase the total target power to 1.2MW. The existing RIL and Linac will be retired, and a new linear accelerator is being built with a new beam transfer line directly into the Booster.

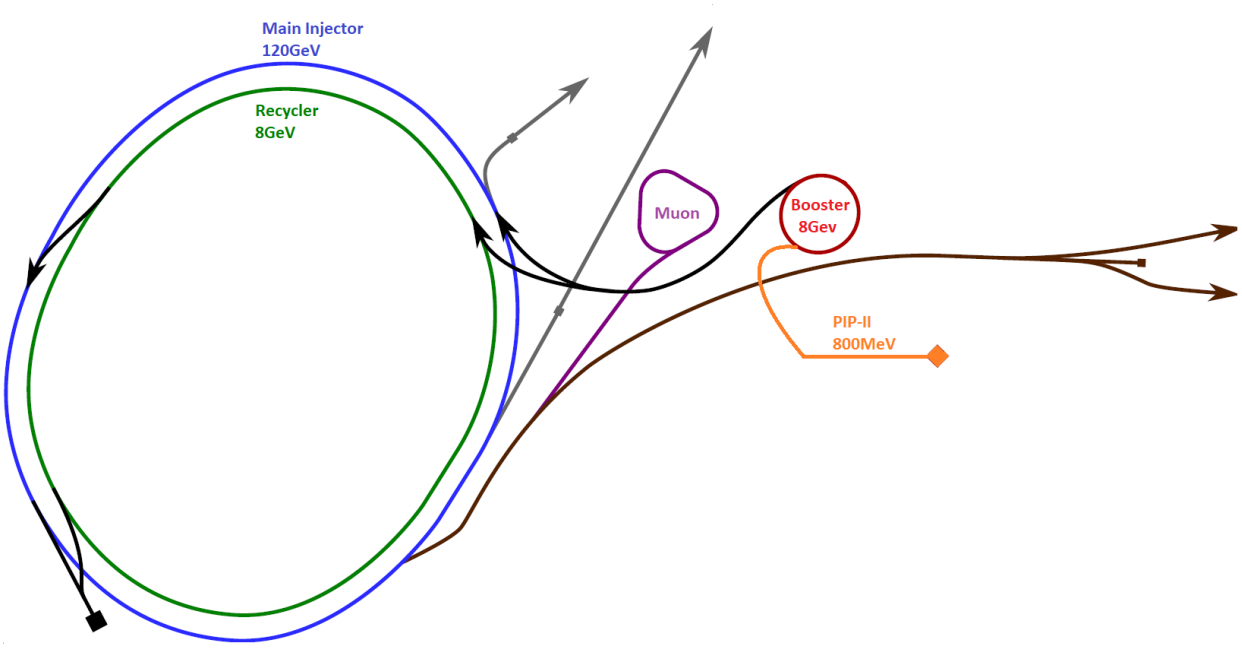

Figure 1-2: Fermilab accelerator complex layout in PIP-II era with new Linac

The original build of Fermilab had a Linac composed of 9 DTL cavities. In the 1990s, the last 4 cavities were replaced with the SCL to increase the output kinetic energy from 200 to 400MeV. [10] The space charge tune shift in the Booster decreases as injection energy increases, leading to a decrease in beam size and losses due to nonlinear field errors throughout the cycle. [13] The PIP-II upgrade seeks to again double the injection energy and is designed to inject 6.5e12 protons into the Booster at 800MeV. [8]

The project also plans to modify the Booster machine frequency from 15 Hz to 20 Hz. This change will result in a steeper momentum time profile, and more RF voltage will be required. The beam current of the new Linac will be 2mA, and the injection period into Booster will be about 550us. The time beam will be present in the Booster decreases from 33ms to 25.55ms.

Table 1-1 Comparison of machine parameters

	Original	Present	PIP-II	
Linac Extraction Kinetic Energy	200	400	800	MeV
Linac operable beam current	25*	27	2	mA
Booster Injection Frequency	30.1	37.9	44.7	MHz
Booster Extraction Frequency	52.808	52.808	52.808	MHz
Booster Extraction Kinetic Energy	8	8	8	GeV
Booster Cycle Time	66.6	66.6	50	ms
Booster Intensity at Extraction	3.50E+12	5.00E+12	6.50E+12	protons
Booster Throughput	1.50E+13	7.50E+13	1.30E+14	protons/second

* This value was estimated

1.2. Objectives and Concerns

The core question that needed to be answered was: can the current infrastructure and cavities handle the change in operating conditions? To realize the PIP-II machine parameters, it was necessary to generate new time profiles, or "programs" for the RF frequency, bias supply, and modulator voltage. Tests were devised to assess the cavity performance, the changes in power demand, the Ferrite Bias Supply (FBS) performance, and the thermal performance of the bus bars. The question below formed the basis of the tests:

- Can the present Booster cavities reliably produce the necessary RF gradient with a 20 Hz rate without sparking or overheating?
- Is the current infrastructure for power delivery sufficiently sized?
- Can the ferrite bias supplies deliver the required current for 20 Hz operation?
- Will the bus bar delivery system for the ferrite tuners overheat?
- Do the bus bar penetrations reach a stable temperature under the melting point of the radiation shielding?

2. Coaxial and Booster RF Cavities

An RF cavity is an enclosed conductive structure, that supports standing electromagnetic waves. RF cavities can in many cases be treated as RLC circuits with spatially varying electromagnetic fields. The quality factor, or Q, of a resonator is a key figure of merit for RF cavities. Q is determined by the ratio between stored energy in a cycle, E_s, to dissipated power, P_D. When the Q of a cavity is higher, it can sustain higher gradients with less power required. Q is defined as

$$Q = \frac{f_{RF}}{\Delta f} = 2\pi f_{RF} \frac{E_s}{P_D} \tag{2}$$

where f_{RF} is the fundamental frequency and Δf is the frequency bandwidth at half power, also known as the 3dB bandwidth. The higher the Q, the more narrowband the response.

The Booster cavities are ferrite loaded dual gap coaxial resonant structures. Ferrites decrease the Q of the cavity because they introduce more power loss to the system, however they also allow for a reliable means of electronically tuning the cavity between 26-54 MHz. The ferrites cores are cylindrical and have high current run through the center inducing a magnetic bias on the ferrites. The bias changes the ferrite cores magnetic domains and decreases the magnetic permeability, μ. This changes the inductance they present to the cavity, and in turn changes the frequency of the cavity. [20] As the tuners are biased more heavily, the RF loss in the tuners decrease, and the Q of the cavity increases. The cavity's Q increases from about 300 to 1100 as the frequency increases from 37.7 MHz to 52.8 MHz.

Fermilab employs many coaxial resonant cavities. The Booster, Recycler and Main injector cavities are all variations on a quarter wave coaxial resonant structure. [1][2]

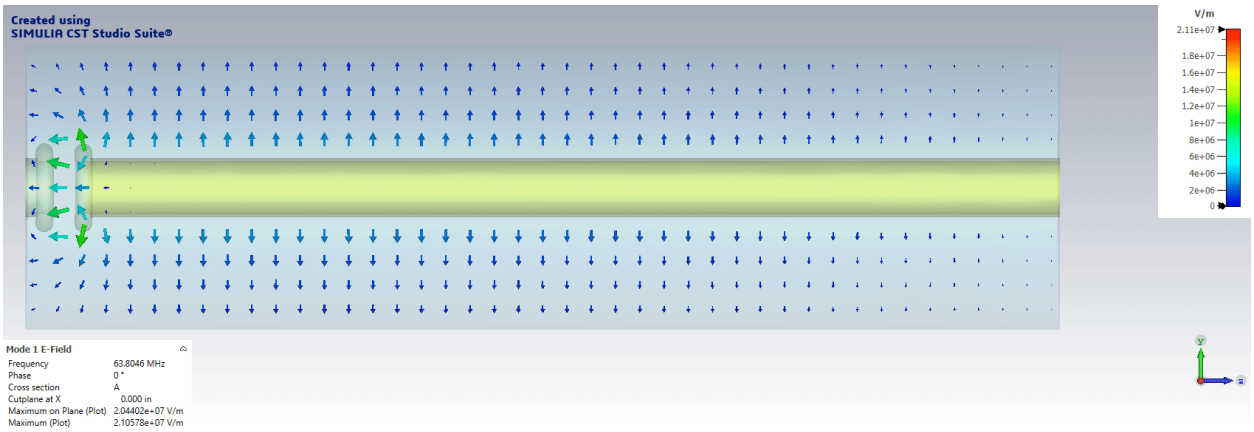

Figure 2-1 Electric field of a simplified quarter wave cavity shown above, on the left is the accelerating gap, and the right wall is the shorted end. Simulation from CST Studios software.

In the quarter wave structure, the electric field is largest in the gap region, and the magnetic field is largest at the outer cavity wall. The boundary condition of the shorted end can be met if two quarter wave structures are arranged back-to-back symmetrically.

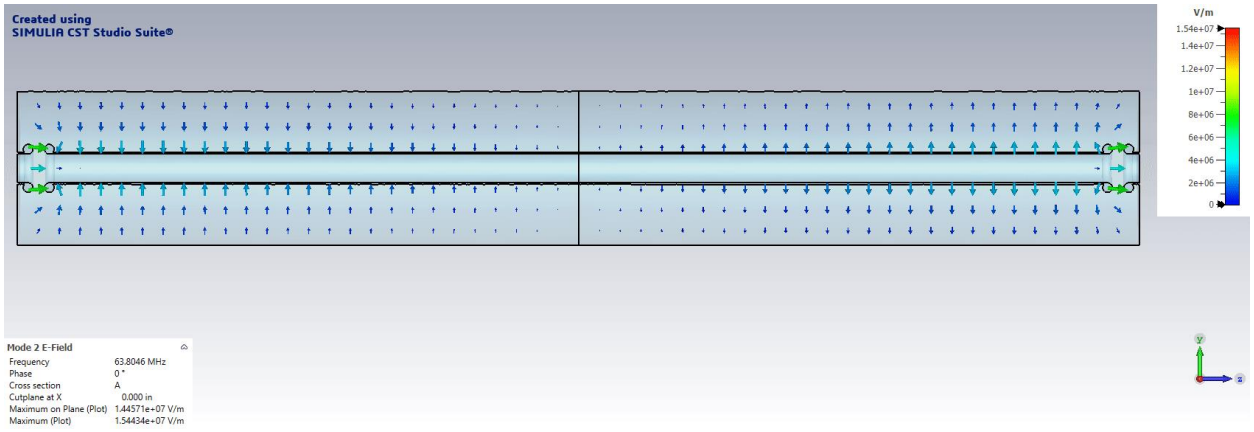

Figure 2-2 Electric field of a simplified dual gap cavity shown above operating in the odd mode. The simulation above displays the gaps at roughly λ/2 apart, with the gap voltage oscillating in phase.

Putting quarter wave cavities back-to-back also creates an even and odd mode near the same frequency. The odd mode has an electric field minimum at the center of the cavity, and a strong azimuthal magnetic field. In the odd mode, the gap voltages are in phase with each other. If a particle traverses the drift region and arrives in the second gap after half of an RF cycles, then it will receive the opposite electric field, and yield no net energy gain. In the even mode, gap voltages are 180

degrees out of phase. If a particle traverses the drift region and arrives in the second gap after half of an RF cycles, then it now receives the proper E-field vector for acceleration. If the particle is traveling at a velocity of βc and the drift length is D, then the optimal drift length will be when $D = \beta\lambda_{RF}/2$. Alternatively, this can be thought of as a gap-to-gap phase advance θ. When θ=180 degrees, the total gap voltage, V_g will be twice that of a single gap V_{1g}. The gaps shorten the θ of the cavity to a non-180-degree values, causing the total gap voltage to be diminished. In the case of the Booster cavity, the θ=140 degrees. [2] [3]

$$V_g = 2V_{1g}sin(\theta/2) \tag{3}$$

The parity of the mode is important for determining the method of coupling. The Booster cavity is an even mode structure, and the Main Injector cavity is an odd mode structure. [6] If the even mode is preferred, capacitive coupling is optimized in symmetric electric fields at the center of the cavity. If the odd mode is preferred, inductive coupling through a magnetic coupling loop, using the prominent magnetic field at the center of the cavity. To prevent the cavity field from being excited in the odd mode, a large inductance is placed at the center line, to move the frequency of the odd mode out of the operating frequencies.

2.1. Booster Cavity

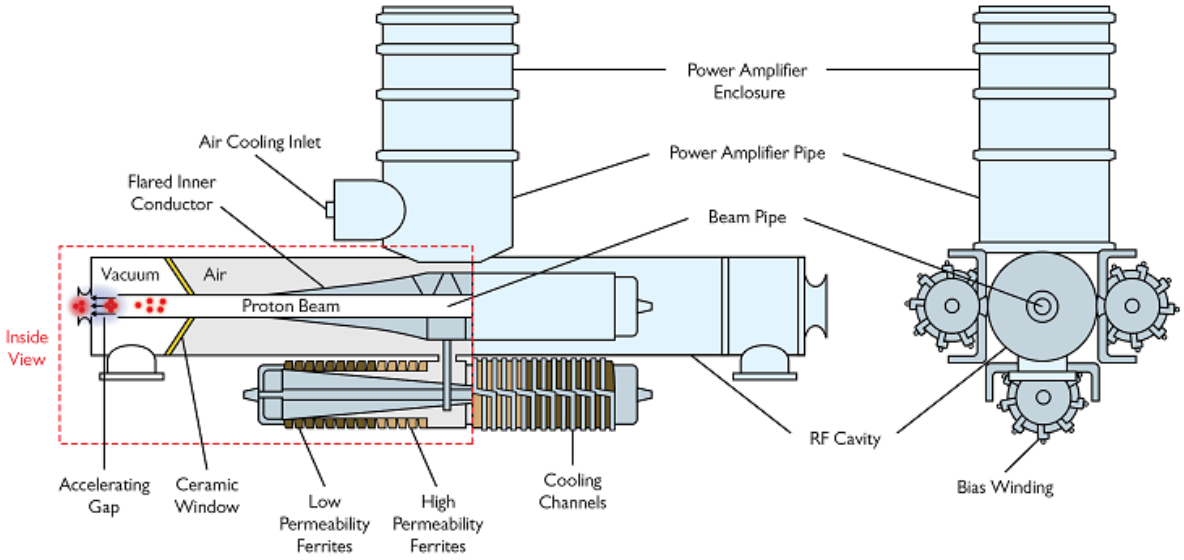

Figure 2-3 Simplified view of Booster Cavity [18]

There are alumina seals “ceramic windows” on both ends to provide a vacuum tight window to the RF gap and beam pipe, while other parts of the cavity are open to air. The vacuum is maintained by a 600L/s diode ion pump.

The inner conductor of the cavity is called the drift tube. The drift tube is tapered to optimize the step-up ratio which is the ratio of the single gap voltage to anode voltage. The step-up ratio is a frequency dependent relationship depending on the impedance of the gap and the impedance of the anode. [6][27] The tapers on each side are joined by a cast copper section called the center casting.

The region inside the taper is a field free region where water cooling is supplied to the center casting. The beam pipe runs through the center of the taper, and the vacuum is continuous throughout.

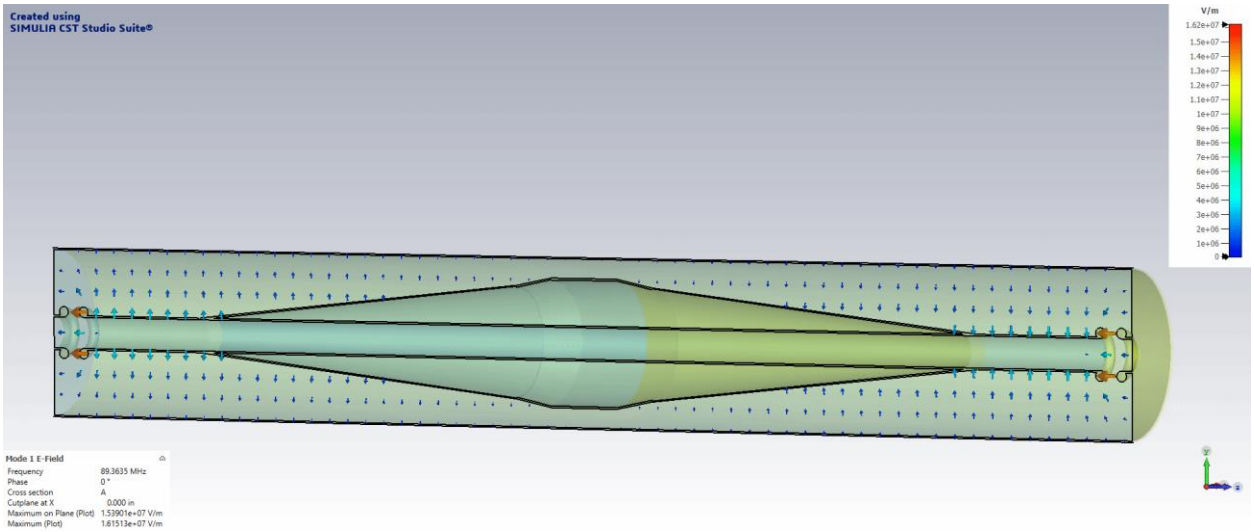

Figure 2-4 Simplified Booster cavity without tuners oscillating in the odd mode.

Each gap is 0.900 inches long, and each gap is slightly offset from the outer cavity wall. Corona rings accompany each gap to minimize sparking. The corona rings also contribute to the field flatness, so any deformation in the area needs to be rectified. [2] The gap-to-gap phase advance θ is 140 degrees. The phase does not change throughout the cycle because the relativistic β and the RF frequency are both functions of the momentum ramp and $\beta\lambda = 5.65\text{m}$ throughout the cycle [22][27]

The gap length L with respect to the wavelength is small, which corresponds to a small variation of the electric field during particle transit through the gap. The transit time factor T_{tr} defines the variation of the electric field during transit through the gap and is assumed to be near 1. [2]

$$T_{tr} = \frac{sin(\pi L/\beta\lambda)}{\pi L/\beta\lambda} \tag{4}$$

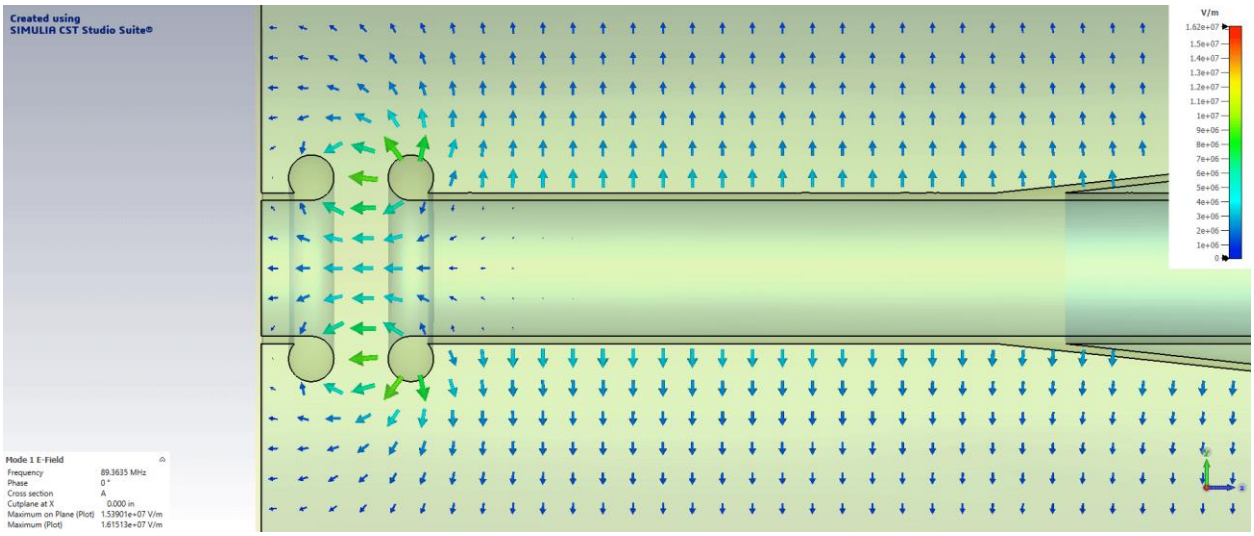

Figure 2-5 Electric field of the upstream gap of the simplified Booster cavity

The center casting is tightly coupled to three ferrite tuners, and to the blocking capacitor of the power amplifier. The tuners are referred to as the front, back, and bottom tuners. They are coupled at the midpoint of the drift tube. The tuners are responsible for changing the frequency of the cavity throughout the ramp. [3]

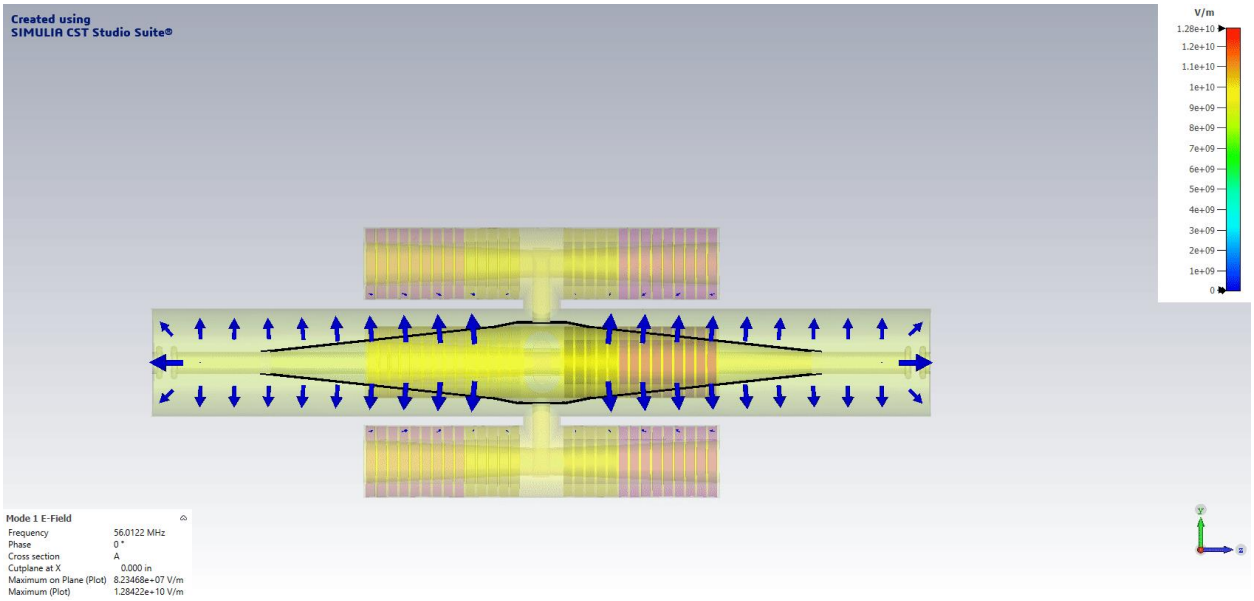

Figure 2-6 Electric field of the simplified Booster cavity with 3 ferrite tuners, oscillating in the even mode.

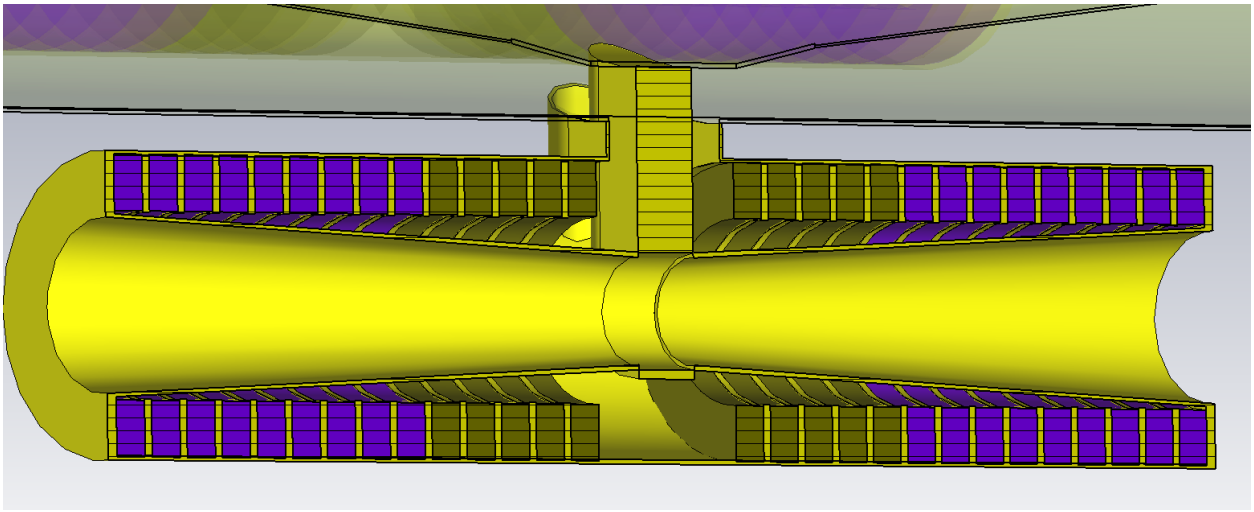

Figure 2-7 Simplified ferrite tuner arrangement green represents high μ, purple represents low μ. Bus bars not shown.

Each tuner is a 41" long coaxial structures filled with Ni-Zn ferrite disks. The ferrites have an 8" outer diameter, a 5" inner diameter, and are 1" thick. There are a total of 28 ferrites per tuner, and they are symmetrically arranged. The outer 9 ferrites are Stackpole Ceremag 2285 ferrites, are commonly called the "low μ ferrites", they have an unbiased μ of about 10.5-12.5. The inner 5 ferrites are Toshiba M4D21A ferrites, are commonly called "high μ ferrites", they have an unbiased μ of about 18-20.

The inner coaxial region of each of the tuners is filled with 10 water cooled bus bars and is commonly called the inner package. The bars form 10 turns that are ramped up to 2500 Amps/turn, creating the equivalent of 25 KAmp of current. As current passes through, an annular magnetic bias acts on the ferrites. [26] In the presence of peak bias, the μ value of all the ferrites approaches about 1.6. [27] The bias current is programmed to optimize the Q at the required frequency.

All three tuners are connected in parallel and powered by a single FBS. On each of the tuners, the bus bars, inner cone region, and outer tuner sections are water cooled with deionized water.

Figure 2-8 Photograph of a tuner's water cooled inner-package bus bars. Photo credit: Fermilab.gov

2.2. Booster Refurbishment During PIP

Proton Improvement Plan, PIP, was an upgrade plan for various elements of the RIL, Linac, and Booster. One of the primary goals was to increase the beam throughput of the Booster. Though the machine frequency was 15 Hz, the RF was only ramped at 7.5 Hz. The Booster cavities and tuners were disassembled, and aged components were replaced.

Building several new tuners required the purchase of ferrites from a new vendor. In a pillbox style test fixture, impedance measurements were taken, and the old ferrites were tested both before and after a bias was applied, to eliminate issues of demagnetization under bias. The low μ cores have a Q of around 280 at a central frequency of 43 MHz. The high μ cores have a Q of around 250 at a central frequency of 35 MHz. [20] The pillbox method can only measure the ferrites without bias.

A half wave resonator test fixture was created in the 1970s to measure the ferrites at 10kA of bias. The test fixture is useful for verifying that the ferrite hysteresis looks acceptable but cannot provide enough current to accurately map the magnetic permeability as saturation is approached. The new vendor was qualified, and some new tuners were installed with the same properties as the old tuners.

A 3.25” aperture cavity was built with a different ferrite arrangement. This cavity was the prototype of a new higher gradient cavity.

3. Booster Infrastructure

The Booster synchrotron has a circumference of 474.2m. The ring is broken up into 24 periods, and there are two buildings upstairs referred to as the east and the west galleries. The east gallery is on top of periods 10-17 and the west gallery is on top of periods 3-20.

Each period contains 2 drift sections and combined function magnets to establish a FDOODFO cell. The two drift regions are 6 meters and 1.2 meters respectively. Within the 6 meter drift sections, 11 of the 24 periods have two Booster RF cavities back-to-back, totaling 22 RF cavities ring-wide. Each RF cavity and its dedicated systems will be referred to as a station. The ring has been in operation since the early 1970's and originally had 16 RF stations, as the beam intensity has increased over the years, so have the amount of RF stations. [7]

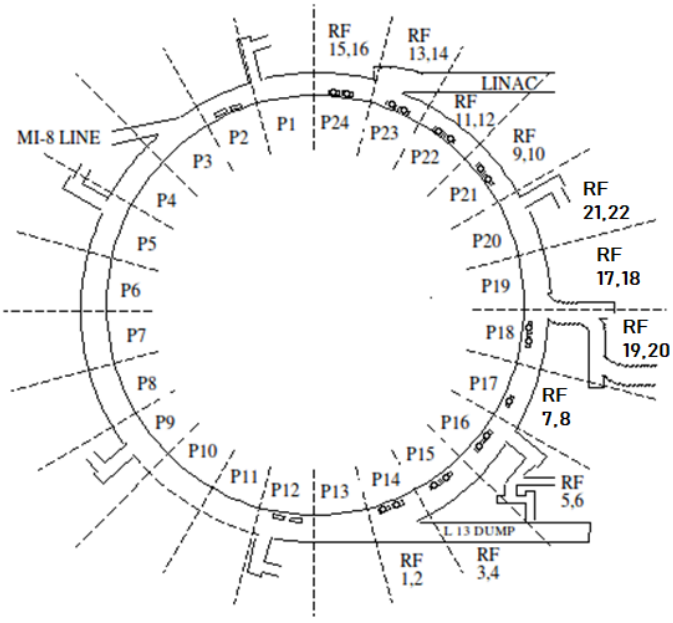

Figure 3-1 Booster tunnel layout, with RF cavity locations marked [7]

3.1. Booster Low Level RF

The LLRF system is responsible for generating and facilitating many of the crucial beam related feedback loops. The system uses a high precision VME-based direct digital synthesizer to generate

the frequency program. This program is amplified and distributed to a centralized location in each gallery. The total group delay of the frequency program is precisely matched for all cavities to 0.1ns.

The phase of all the Booster cavities must add coherently for acceleration, however the Booster cavities are physically spaced throughout the ring. In each gallery, passive phase shifters with matched group delays are utilized to compensate for their variations in tunnel location. The physical spacing of the odd and even cavities are periodic at integer multiples of $\beta\lambda/2$. However, each period has 2 adjacent cavities, so the passive phase shifters compensate by shifting the phase 158 degrees, this aligns the upstream gap of both cavities.

Table 3-1 Tunnel location of each station, and the respective passive phase shift.

East Gallery		
Period	Station	Phase
P14	Station 1	180
P14	Station 2	28
P15	Station 3	0
P15	Station 4	-152
P16	Station 5	180
P16	Station 6	28
P17	Station 7	0
P17	Station 8	-152
P18	Station 19	180
P18	Station 20	28

West Gallery		
Period	Station	Phase
P21	Station 9	0
P21	Station 10	-152
P22	Station 11	180
P22	Station 12	28
P23	Station 13	0
P23	Station 14	-152
P24	Station 15	180
P24	Station 16	28
P19	Station 17	0
P19	Station 18	-152
P20	Station 21	180
P20	Station 22	28

Each station has a feedback loop that locks the phase of the cavity to the phase shifted LLRF. The loop is called the station error loop. A phase detector compares the RF measured on the gap monitor to the input RF and adjusts a dynamic phase shifter in the station's Solid State Driver (SSD) to remove any phase errors generated by the SSD and the Power Amplifier (PA).

3.2. Booster High Level RF

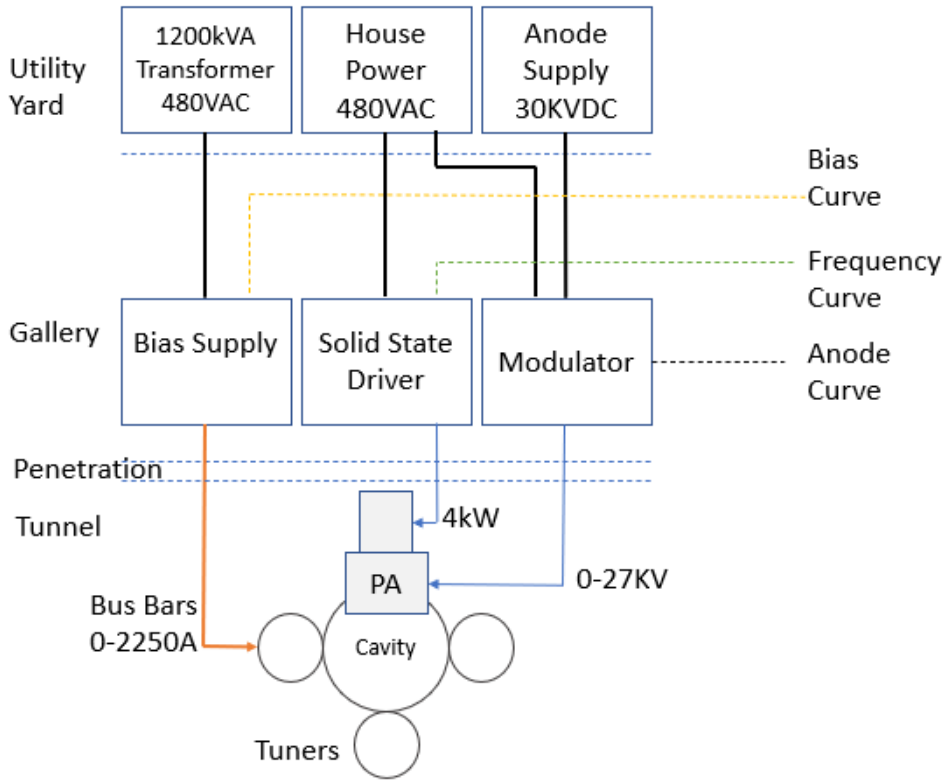

Figure 3-2 Simplified system block diagram of a single station

The PA is directly mounted on the cavity and is a 150kW Y567B tetrode tube, which is a modified Eimac 4CW150000. The anode of the PA is modulated by a high voltage line that is fed through the tuner in the field free region, and into the drift tube and lands at a choke on the blocking capacitor. The modulated high voltage applied to the PA is supplied by a 30kV anode modulator. The cathode of the PA is driven by a cathode resonator, powered by a 4kW SSD. The SSD provides a linear amplification of the phase shifted LLRF signal.

The anode modulator utilizes a tetrode as a switch tube, and its voltage V_m is programmed by the anode program. The screen voltage V_s of the tetrode is biased to 1kV, which reduces the transmitted voltage by 1KV. The anode voltage varies throughout the cycle to shape the RF envelope. [27]

The blocking capacitor is mounted directly to the drift tube at the centerline of the cavity. It is constructed of two concentric cylinders separated by a ceramic with a capacitance of 1200pF. There is a step-up ratio, S, of voltage from the anode voltage to the gap. This ratio varies slightly as a function of the tuner inductance, and ranges from 1.1 to 1.25 per gap. The total gap voltage can be calculated as a function of modulator voltage and gap-to-gap phase advance from equation (4)

$$V_g = 2sin(\theta/2)(V_m - V_s)S \quad (5)$$

The FBS is a high precision shunt regulated DC power supply. As the frequency of the station changes, this supply is responsible for keeping the cavity on resonance by biasing the tuners. The FBS outputs current to the tunnel via a pair of copper bus bars. Each bus bar is constructed of two parallel bars with 0.02" dielectric between them. The entire unit is wrapped in Kapton. Stations 1-16, 19, and 20 have pairs of 4x1/4" bus bars through the penetration.

The power supplies are in the galleries and the location between the galleries and the tunnel is referred to as the penetration. The penetration is filled with 5 feet of polyethylene beads used for radiation shielding. These polyethylene beads have a melting point of about 120C.

The power distribution for the RF systems comes from the east and west utility yards. Each yard has three relevant 13.8KVAC transformers which are for the Anode Power Supply (APS), the bias supply power distribution, and house power. The APS is also in the yard and is responsible for supplying 30KVDC to the modulators. The bias supply transformer is separate from the house power to isolate the heavy load of the pulsed power from the house power.

4. Synchrotron Introduction

A circular accelerator utilizes a magnetic field to develop a closed-loop path allowing for repeated passes or laps through the same beamline components. In the case of the synchrotron, beam is accelerated by RF cavities which provide a kinetic energy gain per rotation. As the beam increases in kinetic energy, the magnetic field is ramped to contain the beam, which is governed by the Lorentz force. The synchronization of the magnets and the RF is the basis of every synchrotron.

4.1. Harmonic Number

RF cavities utilize spatially contained electromagnetic fields to accelerate the particles, utilizing the electric force. The fields oscillate between accelerating and decelerating (along the beam axis) at the RF frequency, f_{RF} , therefore only portions of the RF cycle are usable for stable acceleration. In a synchrotron, the beam must re-enter the same cavities repeatedly. f_{rev} is revolution frequency, or the inverse of how long it takes a bunch of particles to traverse the ring.

If the beam is to arrive in phase with the RF, the relationship between RF and revolution must be preserved, this ratio defines a finite number of stable regions within the machine commonly referred to the harmonic number h. This value determines the number of available "buckets" for the beam. The harmonic number is always an integer to maintain stability in circular machines, if a non-integer value is used, the particles will debunch. [16]

$$h = \frac{f_{RF}}{f_{rev}} \tag{6}$$

The f_{rev} value can be calculated if the particle mass, kinetic energy, and circumference of the machine are known. In the case of Fermilab's Booster, the particle is protons where $m_{proton} = 938 GeV/c^2$, the kinetic energy of the present design is 400MeV at injection and the circumference of the ring, C, is 474.2m.

$$f_{rev} = \frac{\beta c}{C} \tag{7}$$

$$\beta = \sqrt{1 - 1/\gamma^2} \quad where \;\; \gamma = \frac{E_{tot}}{m_{proton}} \tag{8}$$

The machine has been operated with a harmonic number of 84. This value is somewhat arbitrary, but the Main Injector and Recycler require a specific injection frequency, forcing the Booster extraction frequency to match for bucket-to-bucket transfer. To establish the ability to accelerate beam throughout the cycle in a synchrotron, the RF cavity must be able to sweep frequency, this is commonly done via ferrite loaded cavities.

Given equations (6) and (7), the injection parameters can be calculated for the original 200MeV, present 400MeV, and the future 800MeV configurations. In the same fashion the extraction energy of 8GeV can be simply calculated. From this, the following machine parameters are shown in table 4-1

Table 4-1 Machine parameters of original build, present build, and PIP-II

	Original Injection	Present Injection	PIP-II Injection	Extraction	
Kinetic Energy	200	400	800	8000	MeV
Revolution time	2.79	2.22	1.88	1.59	us
β	0.57	0.71	0.84	0.99	
RF Frequency	30.1	37.9	44.7	52.8	MHz

4.2. Accelerating Buckets

As particles pass through a time-varying E-Field, they will receive either an increase or decrease in kinetic energy. The energy gain per rotation can be derived from the Lorentz force equation and the Work-Energy theorem. The energy gain per rotation would then simply be,

$$\frac{dE}{dn} = qV sin\phi \tag{9}$$

When the beam is synchronous to the zero-crossing, $\phi = [0, \pi, 2\pi]$ there is no change in energy. For simplicity, $\sin(\phi)$ can also be defined as $\Gamma = \sin(\phi)$. The determination of which of the zero crossings is stable, is based on the beam's kinetic energy with respect to transition energy. Particle beams have a non-zero momentum spread, and this causes a fractional change in total path length and transit time. The transition-γ or γ_t defines the energy where higher momentum particles transition from having a shorter transit time to having a longer transit time. The effect that an offset momentum has on transit time can be defined by the slip factor η.

$$\eta = \frac{1}{\gamma_t^2} - \frac{1}{\gamma^2} \tag{10}$$

$\gamma_t = 5.446$ for Booster, from 800MeV to 8Gev corresponds to γ of 1.85 to 9.53, Booster will still be crossing transition. From the Hamiltonian and the equations of motion, a stable region of phase space can be defined, called the separatrix. [4] [6] The bucket area, B, of this phase space can be calculated by Equation (11)

$$B = \frac{16R}{hc}\sqrt{\frac{E_{tot}V}{2\pi|\eta|}}\alpha_B(\Gamma) \tag{11}$$

where $\alpha_B(\Gamma)$ is moving bucket area reduction function, which determines how much stable space is available as a function of the synchronous phase. There are several varieties to this function. [4][23][29] Equation (11) from V. Lebedev was used, other versions yield similar results.

$$\alpha_B(\Gamma) = \frac{1-\Gamma}{\left(1+\frac{\Gamma}{2}\right)^2} when\ \Gamma < 1 \tag{12}$$

When $\phi = 0$, $\alpha_B(\Gamma) = 1$ and this is the bucket area of a resting bucket. When accelerating the beam, it is important to conserve the emittance, and typically there is a desired bucket area to emittance ratio.

The two dominant elements in the bucket area equation are the RF voltage and the synchronous phase angle. The next section will discuss the interplay of these two variables.

4.3. New Programs for 20 Hz Operation

Changing the machine frequency to 20 Hz will change all the corresponding RF programs. The new machine frequency will be referred to in angular terms as $w_{ramp} = 2\pi * 20Hz$. Given the machine parameters in Table 1-1 the injection and extraction momentum can be calculated.

Table 4-2 Injection and Extraction momentum of different eras

	800MeV	400MeV	200MeV	
$p_i = \sqrt{E_{inj}^2 - m_{proton}^2}$	1.46E+09	9.54E+08	6.44E+08	eV/c
$p_f = \sqrt{E_{ext}^2 - m_{proton}^2}$	8.89E+09	8.89E+09	8.89E+09	eV/c

The momentum time profiles were created assuming a sinusoidal momentum ramp. [5]

$$p(t) = \frac{p_f + p_i}{2} - \frac{p_f - p_i}{2} cos(w_{ramp} t) \tag{13}$$

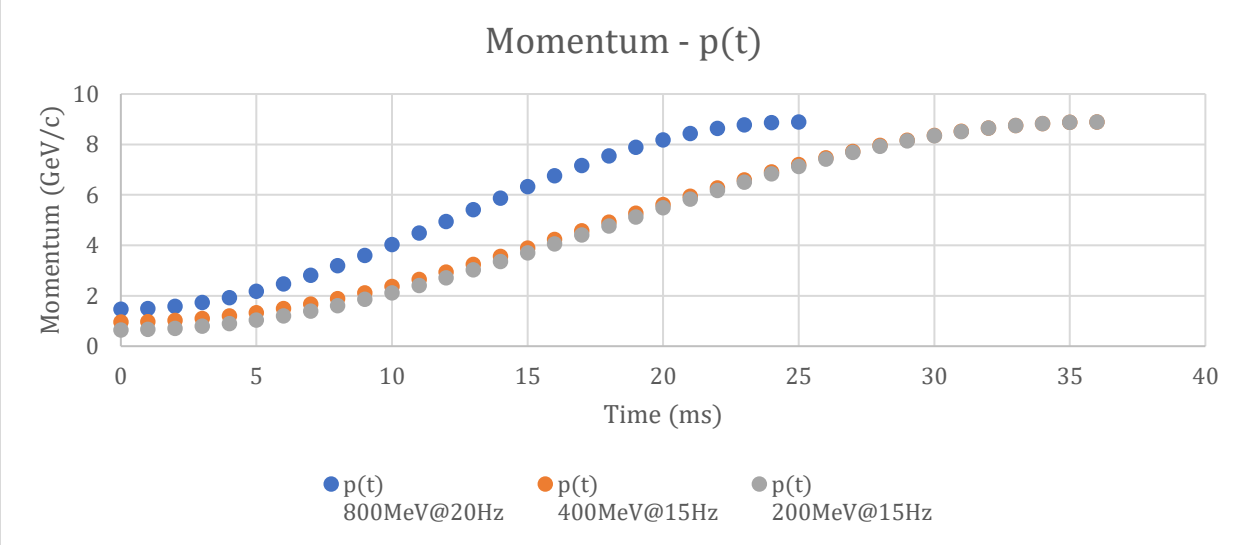

Figure 4-1 Momentum time profile for different operating conditions, note the dominant factor is machine frequency

With a harmonic number of 84 and the given ring circumference of 474.2m from Table 1-1, the frequency program was calculated. The momentum time profile, Equation (13), can be used to calculate β, and the harmonic definition, Equation (6), can be solved for frequency. This program determines what RF frequency is needed to align with the momentum time profile.

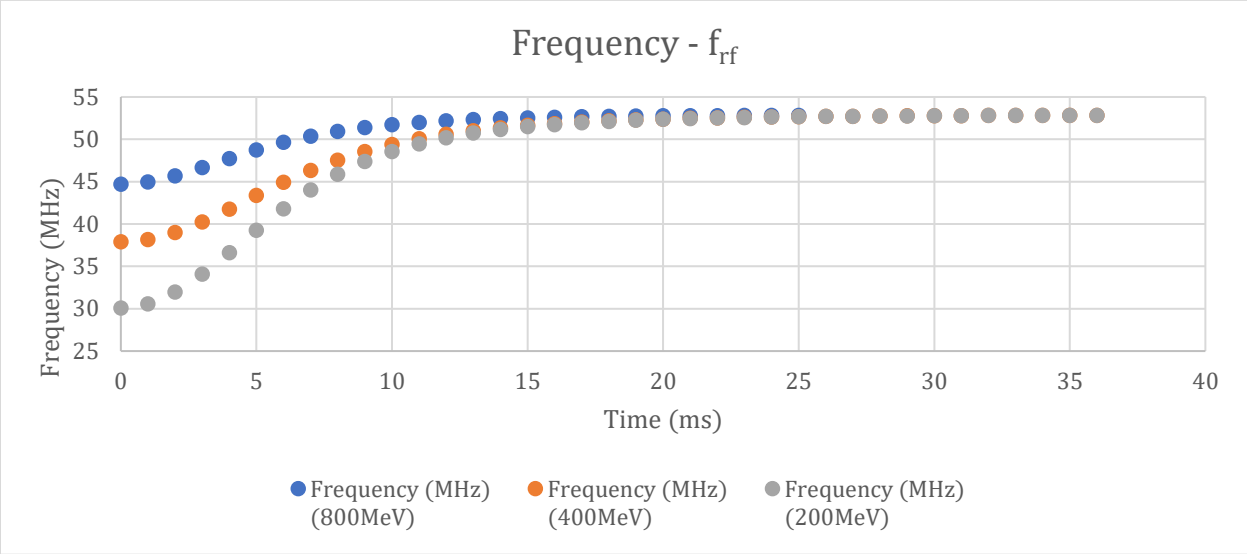

Figure 4-2 Injection frequency of the original design had a span of 23 MHz, PIP-II has a span of 9 MHz

In order for beam to stay on a fixed orbit, dE/dn can be defined in terms of momentum.

$$\frac{dE}{dn} = \frac{p(t)}{E_{tot}}\frac{dp}{dn} \tag{14}$$

To incorporate the periodicity of the acceleration, define $dn = f_{rev}dt$. Setting the energy gain from the Lorenz force, equation (9) with energy required to stay on momentum, equation (13)

$$\frac{dE}{dn} = qVsin\phi = \frac{p(t)}{E_{tot}}\frac{1}{f_{rev}}\frac{dp}{dt} \tag{15}$$

The maximum energy gain will occur when $\phi = 90$. Solving equation (15) for this value, allows calculation of the minimum required RF voltage V_{min}. These values would only apply to a perfectly synchronous particle and does not consider emittance conservation. [2]

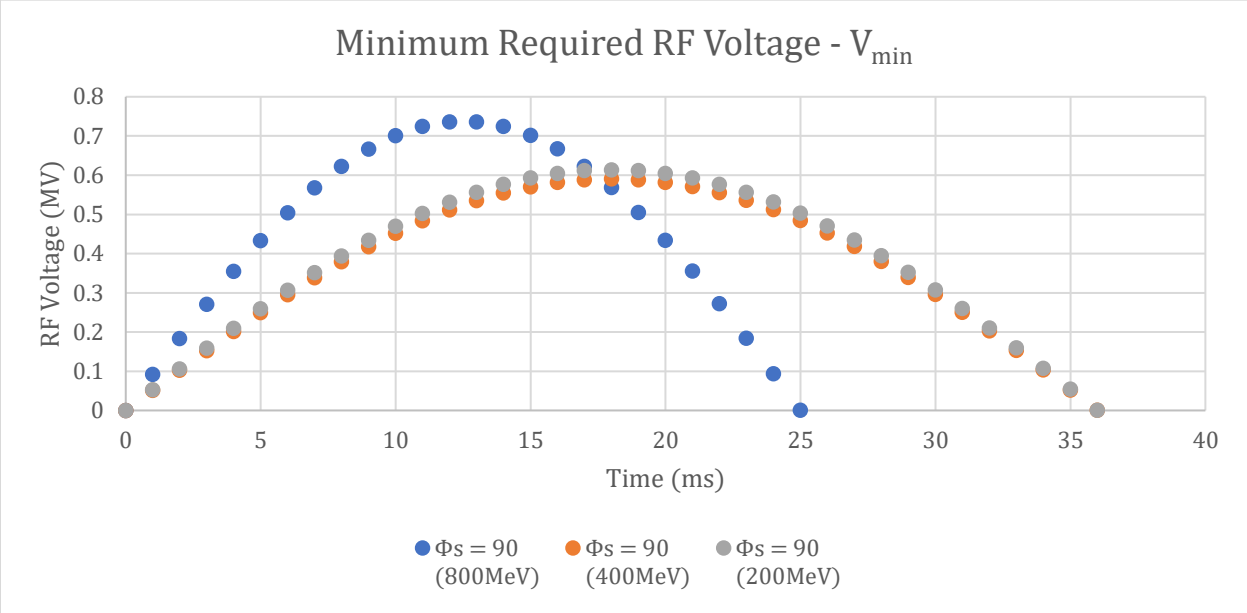

Figure 4-3 The 800MeV V_{min} increased due the higher dp/dt from 20 Hz ramp. If injection energy alone was increased, V_{min} would be lower than the 400MeV case.

In practical application a stable bucket is required, and the conservation of longitudinal emittance is important. One way to approach this is to fix a bucket area to emittance ratio. The desired ratio in this case is 2.3, with an assumed Gaussian emittance of 0.063eV s. Rearranging equation (11) to solve for V_{RF}

$$V_{RF} = \frac{2\pi h|\eta|}{E_{tot}}\left(\frac{hcB}{16R\alpha_B(\Gamma)}\right)^2 \tag{16}$$

Γ can be solved for by setting equation (16) equal to V_{min}. After calculating the roots of this equation, the calculated Γ can be re-written in terms of ϕ_s and (π-ϕ) can be applied for post transition.

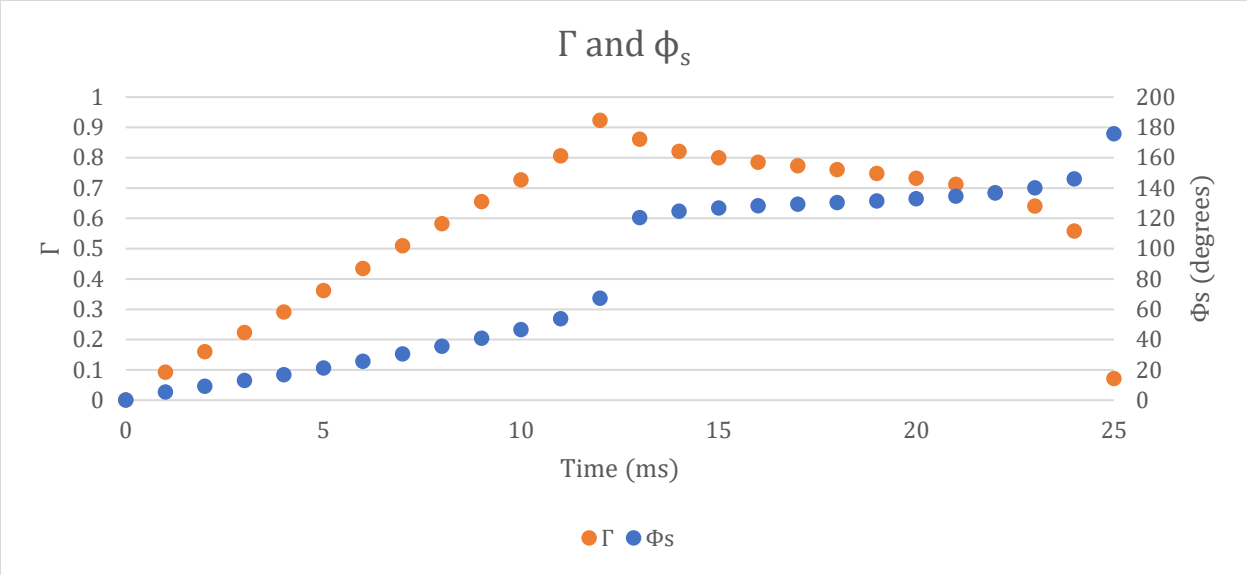

Figure 4-4 The interplay between Γ and RF voltage allows for the bucket area ratio to remain constant

V_{RF} can then be defined with a stable bucket area to emittance ratio [1] [23]

$$V_{RF} = \frac{V_{min}}{\Gamma} \tag{17}$$

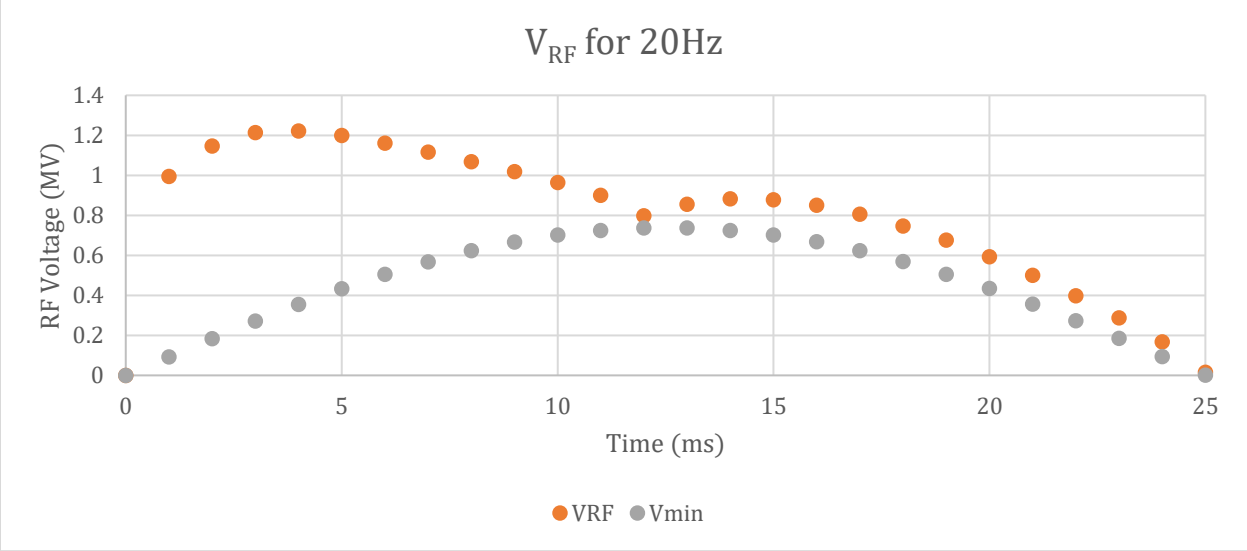

Figure 4-5 V_{RF} max value is at 4.75ms, the V_{min} max value is at 12.7ms. The V_{RF} max value is driven by emittance conservation, rather than the peak of dp/dt.

The 20 Hz V_{RF} program defines a peak ring-wide voltage of about 1.2MV. To achieve this, 16 of the legacy stations need to provide 50KV per station, and the 6 new cavities which will replace 6 legacy stations will need to provide 66.7KV per station. To scale the required voltage, the legacy V_g was set to $V_{RF}/24$. The required modulator voltage was then calculated from equation (5) to create the anode program.

In present operation, a peak ring-wide voltage of 920KV is needed. This relies on all 22 stations to operate at 42KV, or for 20 stations to operate at 46KV, with 2 stations available as hot spares. The 20+2 redundancy configuration has improved the reliability of the machine and minimized downtime due to RF issues. With the higher demand for RF in the 20 Hz era, there will no longer be cavity redundancy, and this will impact long-term availability of the machine.

4.3.1. Bias Program

The bias program is responsible for keeping the cavity at high Q throughout the frequency sweep of the system. To measure the Q and frequency of the cavity over a range of currents, a network analyzer was connected to measure the S21 with port 1 into a PA with a 1" coupling loop, and port 2 at the output over the gap monitor.

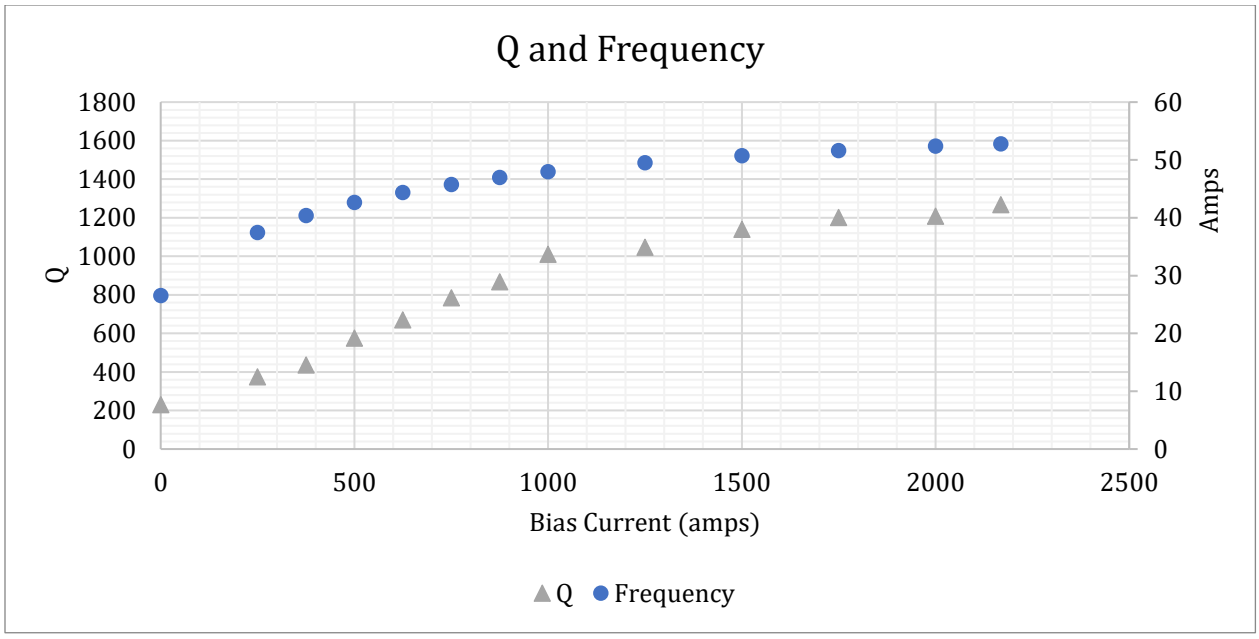

Figure 4-6 Test stand Q measurements of a legacy station. As bias current is increased, Q increased.

The bias program created was extrapolated from S21 summarized data shown in above, and manually tuned to minimize phase errors.

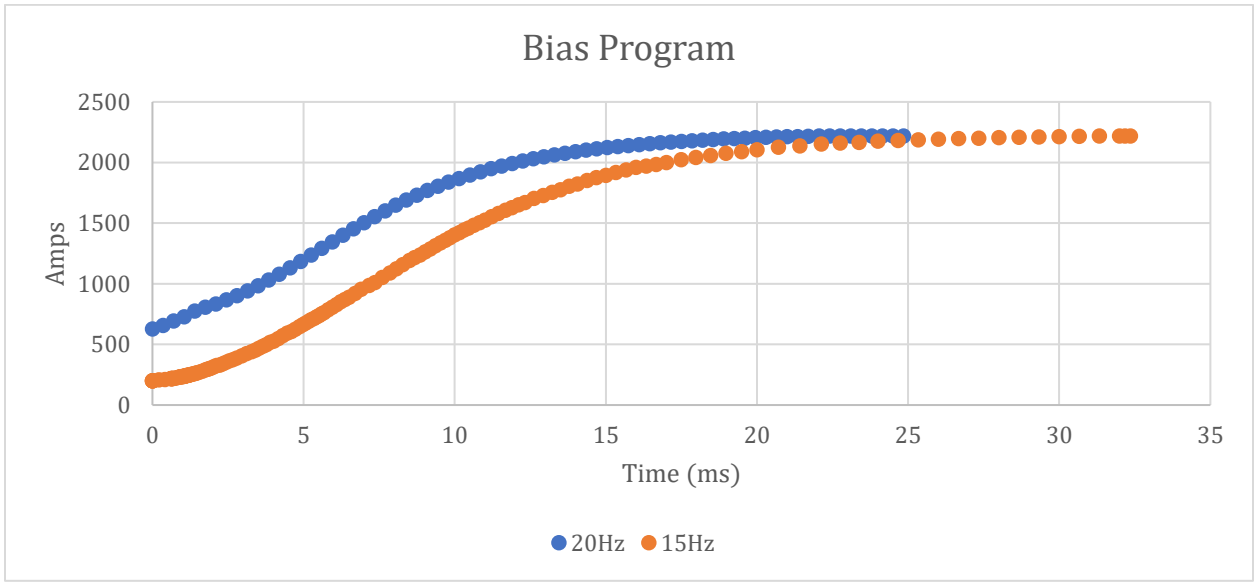

Figure 4-7 Bias program based off the frequency program shown. The higher injection frequency raises the initial current by 420 Amps

Each station has a dynamic feedback loop called the cavity tuning loop, which is summed with the incoming bias program. This loop compares the phase of the RF drive measured on the PA cathode monitor against the phase of the cavity gap monitor, measured from a transformer coupled capacitive

pickup on the cavity. If the phases are misaligned, this loop will increase or decrease the FBS output current depending on the direction of the error. This feedback loop allows for all stations to operate off the same bias program.

The FBS are required to ramp down in-between cycles and have a limited positive and negative slew rate. If a ramp program exceeds this rate, the supply will not be able to regulate, and may oscillate. The slew rate is bounded by the maximum and minimum output voltage of +35 to -15V.

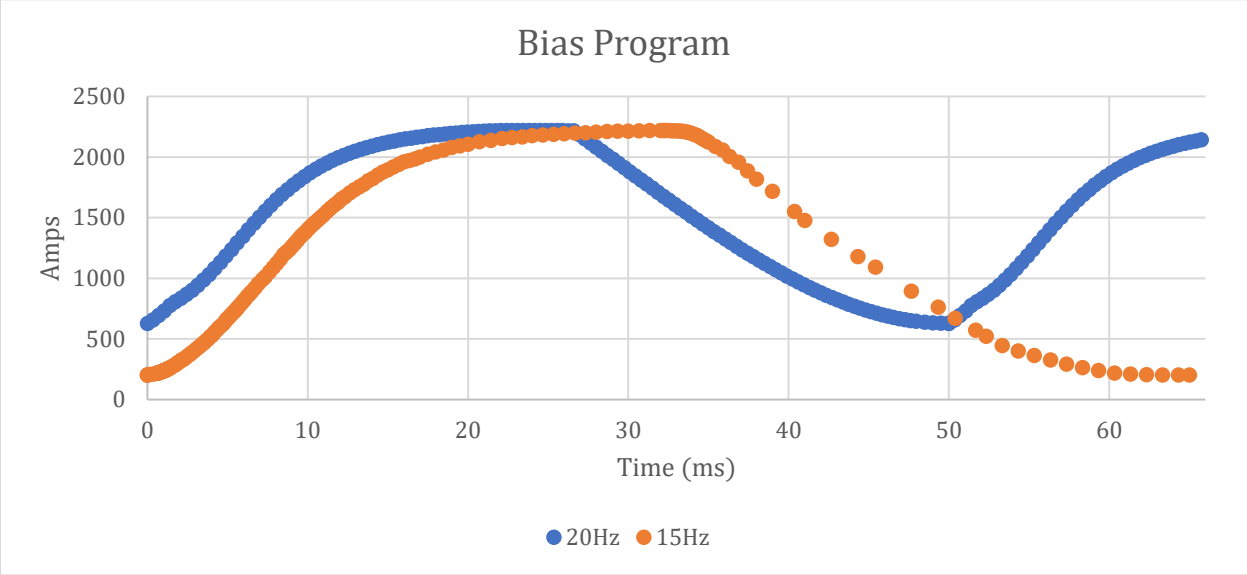

Figure 4-8 Bias program of 20 Hz system compared to 15 Hz

At 20 Hz, the bias supply was not capable of ramping down to zero and always stayed above 620 Amps. Root Means Squared (RMS) current allows for a direct thermal equivalent to DC,

$$I_{RMS} = \sqrt{\frac{1}{T_2 - T_1}\int_{T1}^{T2} I^2(t)\, dt} \tag{18}$$

The I_{RMS} of the 15 Hz program and the 20 Hz program were compared, predicting an increase of 25% in current. Additional thermometry was added in the predicted hot spots.

5. Testing

With the newly derived programs for 20 Hz operation, verification testing of the cavities and peripheral equipment was necessary. The first tests were completed in a dedicated test cave decoupled from the accelerator complex. The second batch of tests were conducted in the active accelerator during dedicated test time.

5.1. Test Stand Setup

Main Injector and Booster cavities have historically been tested in the in the MI60 service building, at the MI test stand. The cavity would be in an interlocked cave and the test equipment was in the gallery. The test cave could only accommodate one cavity at a time, and the electronics were shared. Frequent reconfiguration was needed, driven primarily by operational needs.

For the 20 Hz testing, a parallel signal path was built into the cave with its own fully integrated Booster test stand. Room was cleared out in the test cave so that both a MI cavity and a Booster cavity could be installed simultaneously. The new Booster test stand had a dedicated LLRF system, solid state amplifier rack, controls rack, and timing hardware. It shared an anode supply, bias supply, and anode modulator with the MI test stand.

Figure 5-1 New Booster test stand at MI60

Timing for the present complex is based off the Booster's 15 Hz which is not line locked, rather based off a magnetic field measurement from a reference magnet. In PIP-II era, Boosters magnet girders will be modified to have different RLC properties that align with 20 Hz. At the time of testing these modifications had not been started, and 20 Hz triggering was not available anywhere onsite. The timing of the accelerator complex is based off a system called TCLK, which broadcasts timing events, systems then receive the signal and decode it looking for events to trigger from. A new timing event, called the $BA, was created to include a novel global 20 Hz event. The event was self-referential and not locked to the line power nor the Booster magnets. This new timing event allowed for synchronization of the data acquisition systems, and the program triggers.

The LLRF system was a VME based Direct Digital Synthesizer. The system was identical to the operational system but was then modified to be able to run at a 20 Hz rep rate. The VME system was responsible for providing the frequency and bias programs.

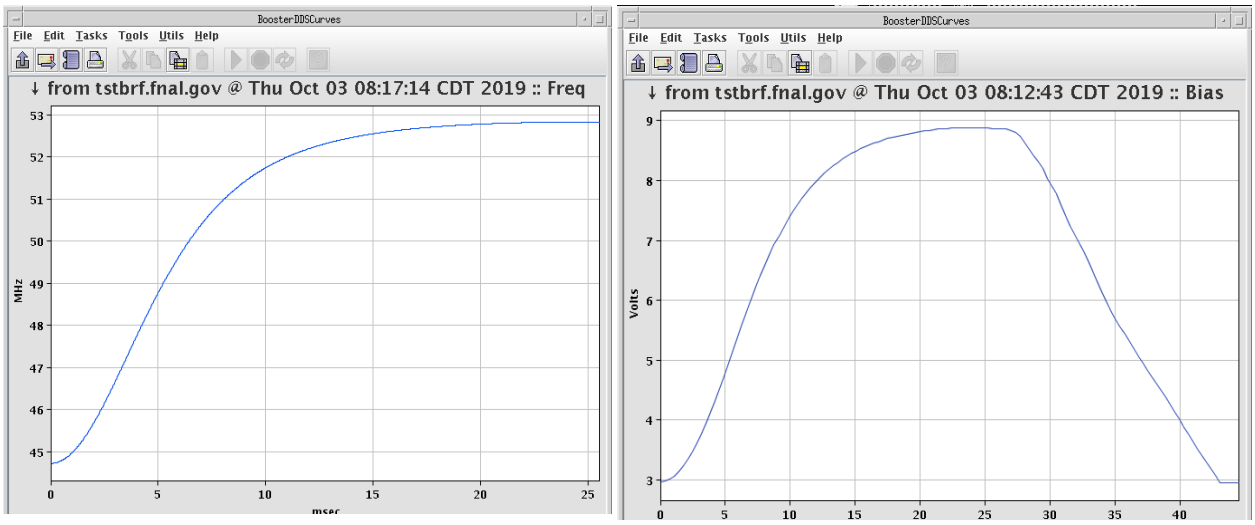

Figure 5-2 Screenshot of frequency and bias programs.

The anode program derived earlier was modified to include a larger bucket area post transition and to include an additional 2ms injection window while the cavity was at 44.7 MHz. The anode program (APG) and SSD Program (CIG) were programed onto the CAMAC 473 ramp cards.

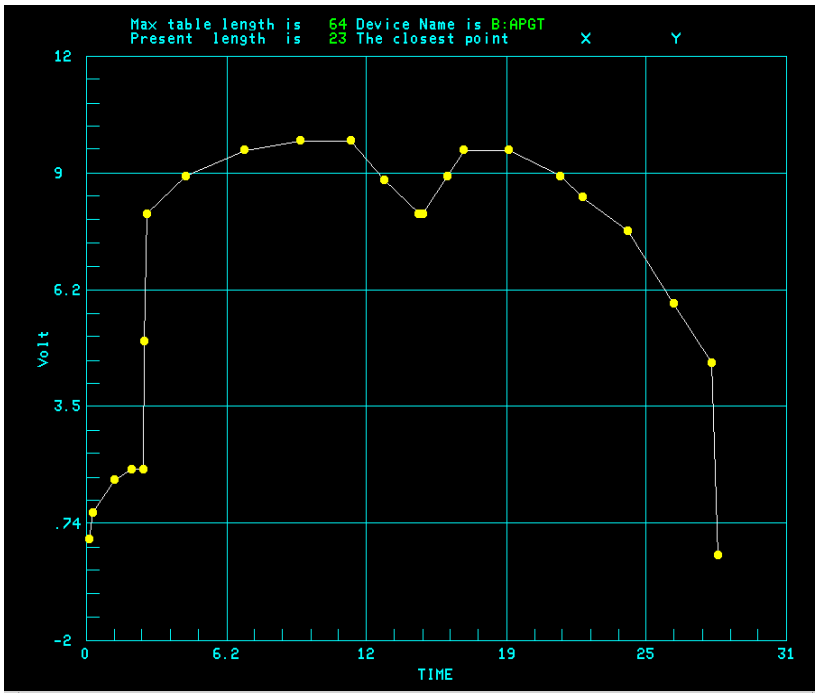

Figure 5-3 Anode program (APG) shown above, the ramp was extended by 2ms to emulate an injection interval.

5.2. Measurement Setup

Each cavity contains 4 internal thermistors, one located in the center casting, and one on each stem of the front, bottom, and back tuners. These 4 thermistors are installed in every cavity and are actively read back through the ACNET control system. RF fields would prevent active thermometry from working in some critical places. For these measurements, RF was turned off and they were measured using a Fluke 80T-150UA contact thermometer connected to a DVM. For each side, a measurement of the ceramic window, stainless steel collar and a beam tube was obtained, as is shown in Figure 5-4

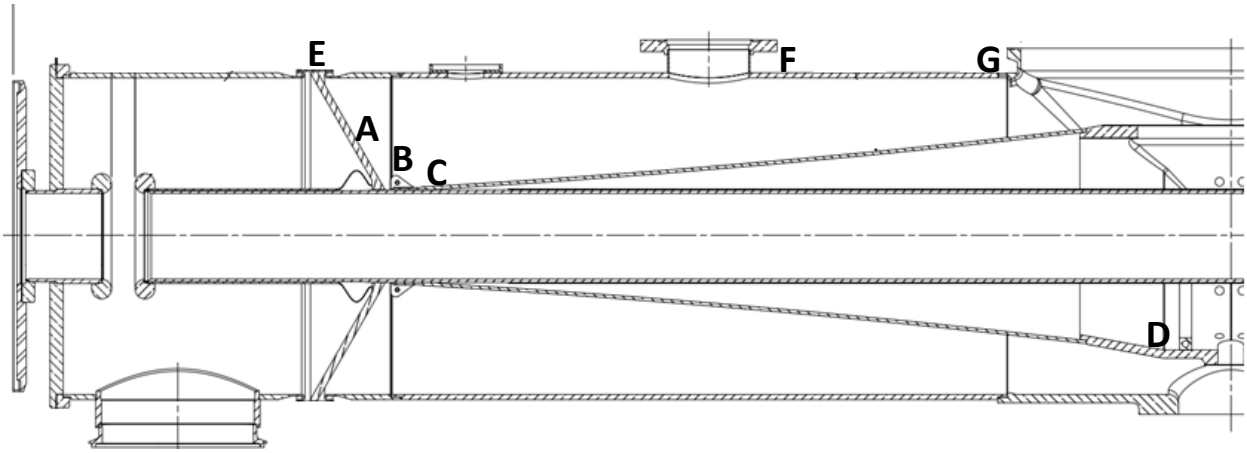

Figure 5-4 Above is a cross section of the left half of a Booster cavity, measurements are mirrored on both sides. Thermometry points A, B, & C correspond with ceramic window, stainless steel collar, beam tube. Point D is center casting thermistor that read back through ACNET. E, F & G correspond with the ceramic outer ring, the 84 MHz damper port, and the PA flange.

In the test cave only, the cavities were equipped with additional thermistors mounted externally on the upstream and downstream ends of bias tuners, the cavity body itself, and the outlet air temperature. Temperature labels were also added to each of the tuner stems on their outer edge, the temperature labels are one time use, and record the highest temperature in 5-degree intervals.

For the in-situ Booster measurements, the AC power was monitored. Each gallery's 3-phase 480VAC main breaker is equipped with a PowerPact RG-1600 main breaker, which reports back real, apparent and reactive power in real time via the ABB PowerLogic system. Thermistors were added

to the bus bar penetrations inside the polyethylene beads that were used for radiation shielding. This area has no air flow and has the longest duration to reach thermal equilibrium.

5.3. Test Stand Data

The test cave was configured for operations in both 15 Hz and 20 Hz enabling direct comparisons. First, a low gradient and low repetition rate of 0.1Hz was established to verify the amplifier programs, and that the cavity was tuning correctly.

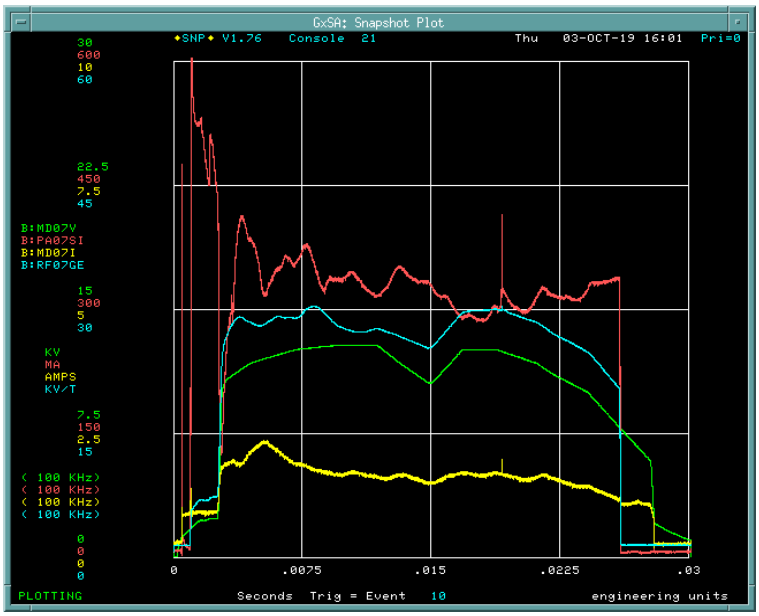

Figure 5-5 RF parameters plotted at low gradient of 30KV

With the cavity at low gradient, the repetition rate was slowly increased up to 20 Hz. The timing, anode program, and the bias program during the cycle looked acceptable, however the bias current between cycles was not regulating as repetition rate was increased. The negative slew rate of the FBS was not fast enough, indicating that more tuning of the program was required. The modified program resulted in the current never decreasing below 620Amps.

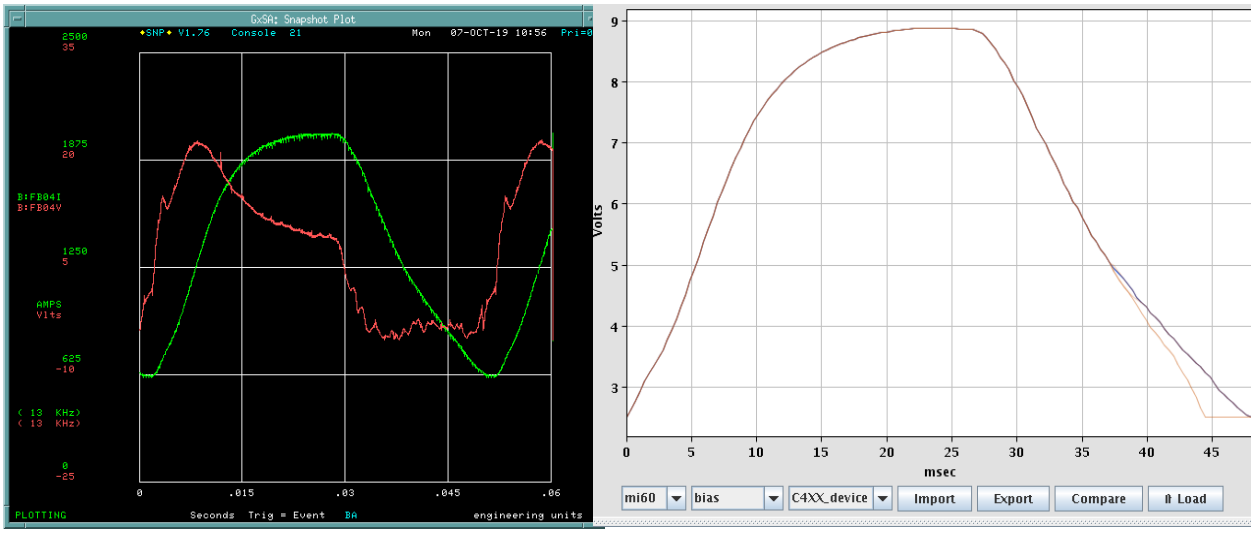

Figure 5-6 Left screenshot of bias voltage and current after tuning, right screenshot shows the increase adjustments to the program

After prolonged testing at low power, the modulator voltage was increased in 3KV steps from 12KV to 24KV. Thermal measurements were conducted at each voltage, after about 4 hours at each value. A peak gap voltage of 50KV was reached, and thermal measurements are shown in figure 5-7.

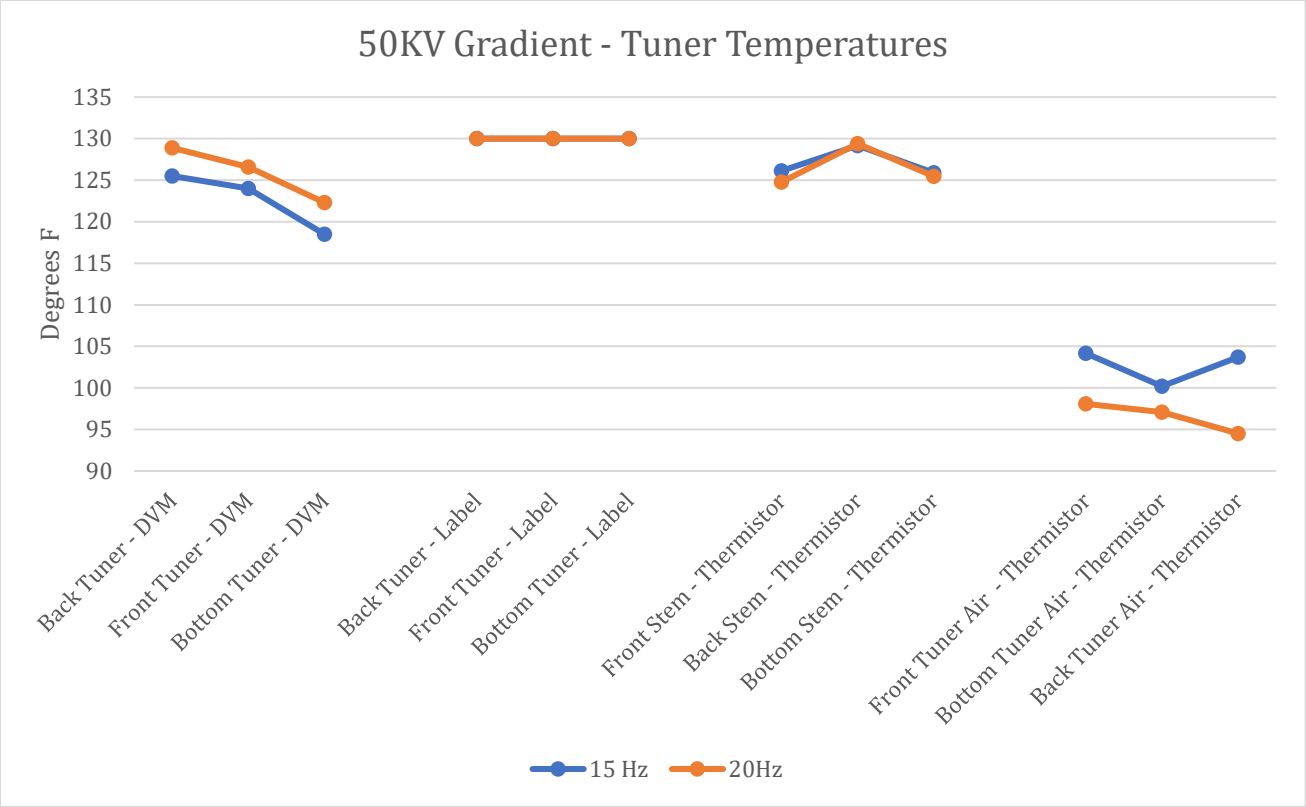

Figure 5-7 With a 50KV gap, the tuner measurements shown above show 15 Hz and 20 Hz values are within 5 degrees.

The inner package and the outer conductor of the ferrites are water cooled and appear to have adequate flow. The tuner temperatures were comparable between the 15 Hz and 20 Hz modes of operation. This was corroborated by the tuner stem temperatures measured on the thermistors.

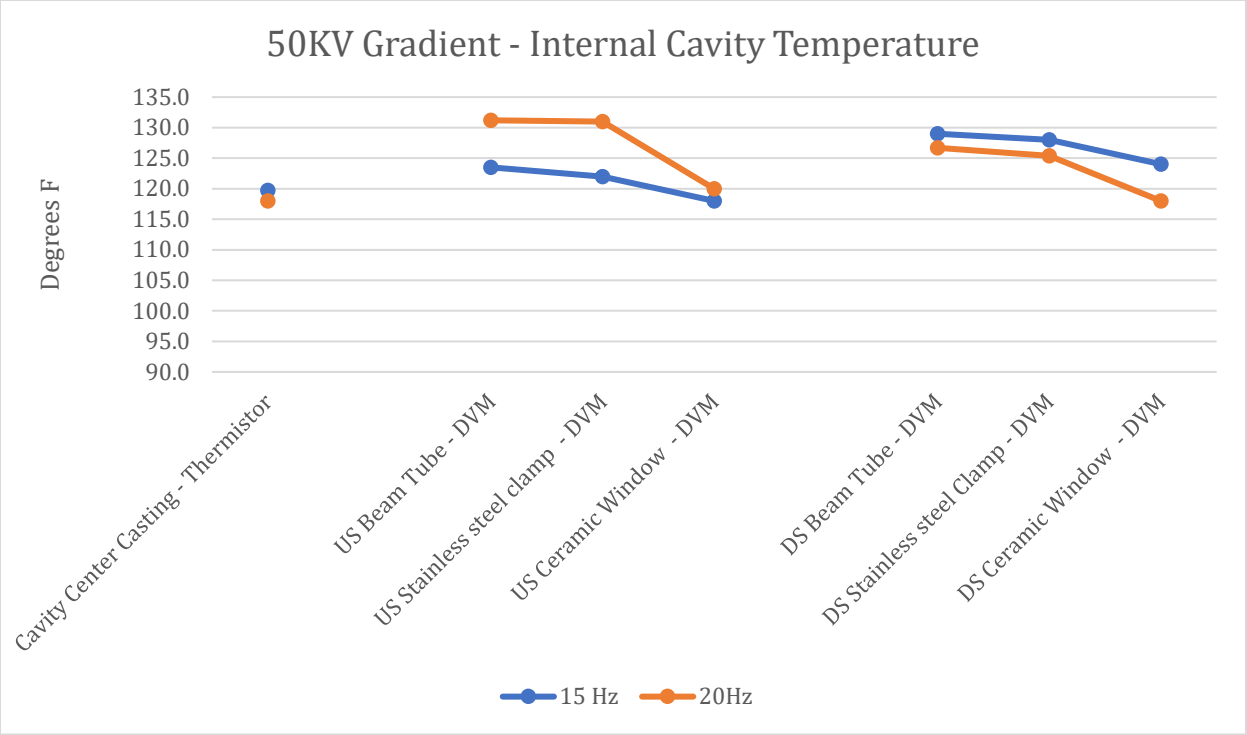

Figure 5-8 Internal cavity temperatures

The internal measurements are useful to identify high RF losses. The primary method of cooling for the inner components is forced air. The internal temperatures are comparable in both operating modes. The ceramic windows overheating was the primary concern, specifically at the mechanical junction by the stainless-steel clamps. However, the temperatures were stable, and no thermal run-aways were observed.

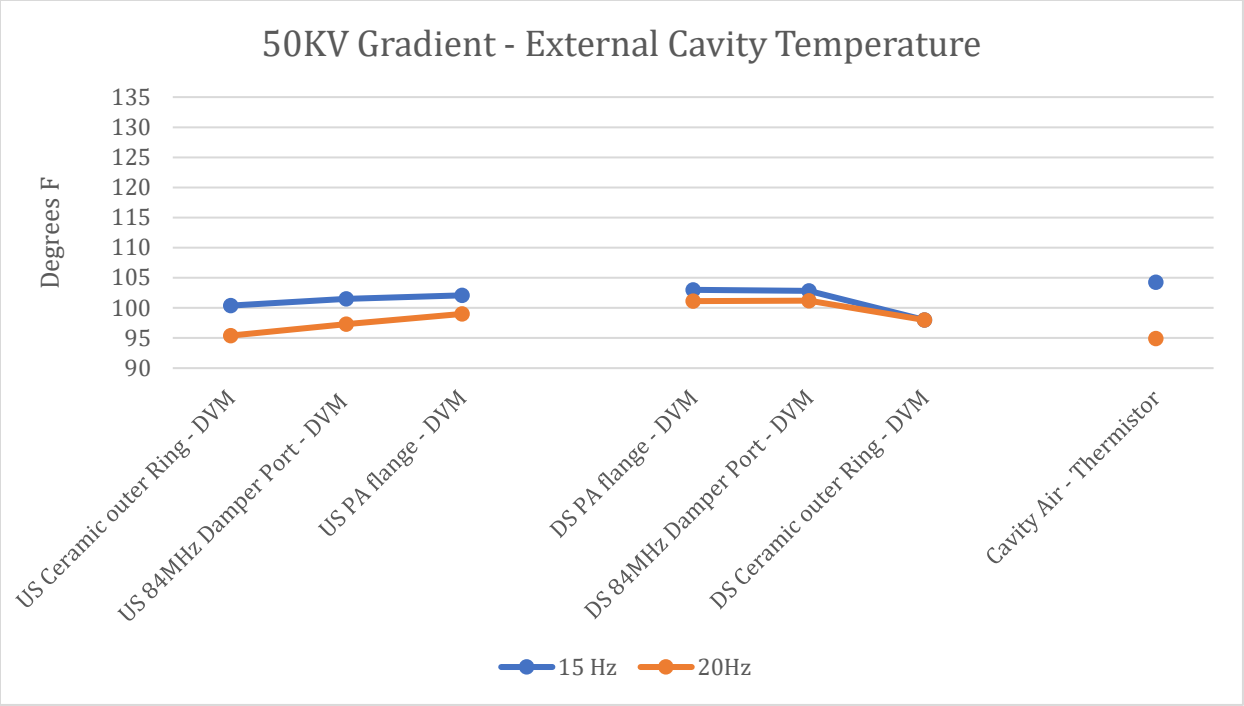

Figure 5-9 Exterior cavity measurements were comparable between modes.

The exterior cavity measurements are helpful to identify new thermal gradients caused by the change of frequency. A large thermal gradient over the ceramic would be bad for its structural integrity. The internal temperatures are comparable in both operating modes.

In order to conduct calorimetric measurements on the tuner, the water path of the tuners, center castings were diverted to a flow meter and an RTD, this allowed for the isolated measurements of power dissipated to water. To calculate the power dissipated into the water P_W in kilowatts, it is necessary to know the fluid type, the change in temperature between inlet and outlet water ΔT, measured in C, and the flow rate Q measured in GPM. In the case where the signal is pulsed, to calculate the power it is also necessary to know the duty factor DF. The duty factor of both 15 Hz and 20 Hz is the same.[17]

$$P_w = \frac{Q\Delta T}{3.79DF} \tag{19}$$

Table 5-1 Calorimetric measurement comparison of 15 Hz and 20 Hz at 45KV gap voltage after 2 hours to ensure thermal equilibrium

	20 Hz		15 Hz		20 Hz-15 Hz
	Flowrate (GPM)	Power (kW)	Flowrate (GPM)	Power (kW)	Delta Power (kW)
Central Casting	.85	0.61	0.855	0.654	-0.044
Downstream Back Tuner	1.5	2.84	1.46	2.67	0.17
Upstream Back Tuner	1.5	2.86	1.51	2.77	0.09
Upstream Front Tuner	1.5	2.84	1.48	2.89	-0.05

The test cave does not use standard bus bars and instead uses eight 500MCM cables, which has a much higher ampacity than the Booster 4" bus bars. This effectively isolates ohmic losses in the power distribution and shows the ohmic losses in the tuner bus bars did not change significantly.

5.4. Tests Setup Used on Current Booster

20Hz testing on the active Booster required dedicated study time and was conducted during a long shutdown. After the cave testing was completed, the modified LLRF system was installed into the existing Booster, temporarily replacing the systems native LLRF system. All other programs were transferred into the existing infrastructure and set to trigger on the new timing event. The test stand was built to directly emulate the existing Booster, so transferring the other programs was straightforward. The programs from the test stand were reverified at low gradient.

5.4.1. Pulse Multiple Bias Supplies

The bias supply power distribution is divided by east and west galleries. There are 12 bias supplies in the west gallery, and 10 bias supplies in the east gallery. Each yard has a 1200KVA transformer, with a three phase 13.8KVAC to 480VAC step down transformer. The only load on the east gallery

transformer is the 10 FBS. The east gallery was chosen for the test because the west gallery still had 92KVA of other loads on the transformer and would cause problems for the other systems.

The power consumption of the bias supplies was a concern, due to the higher RMS current of the new programs. After verifying the bias current could tune with RF on a single station, all of the east gallery bias supplies ran with the new bias program. Critical parameters such as power draw and temperatures were monitored. The power draw in the utility yard was monitored on the ABB PowerLogic system. Power measurements with the 15 Hz and 20 Hz bias programs were completed back-to-back, with time allocated for cool down.

Table 5-2 Comparison of measured power with 10 stations operating

	15 Hz	20 Hz
Real (kW)	277	337
Reactive (KVar)	1049	1199
Apparent (kVA)	1086	1246

	15 Hz	20 Hz
Current (Average)	1376	1589
Current A RMS	1344	1635
Current B RMS	1404	1604
Current C RMS	1379	1525

At 20 Hz rep rate, there was an increase in the apparent power in the gallery by 160KVA, pushing the total value to 1246KVA. Continuous operation under these conditions was not acceptable and had potential for overheating. Each station has a fused disconnect, which is fused at 200 Amps, and the increase in power would have caused them to operate very close to 80%, the Fermilab site standard for loads.

The power factor of the gallery was about 0.27 at 20 Hz, this is about the same as the value at 15 Hz but does provide an opportunity to increase efficiency. The current on the A-phase increased 22%, corresponding with an increase of ohmic losses by 48%. IR thermal imaging was also conducted on the outside of the yard transformer.

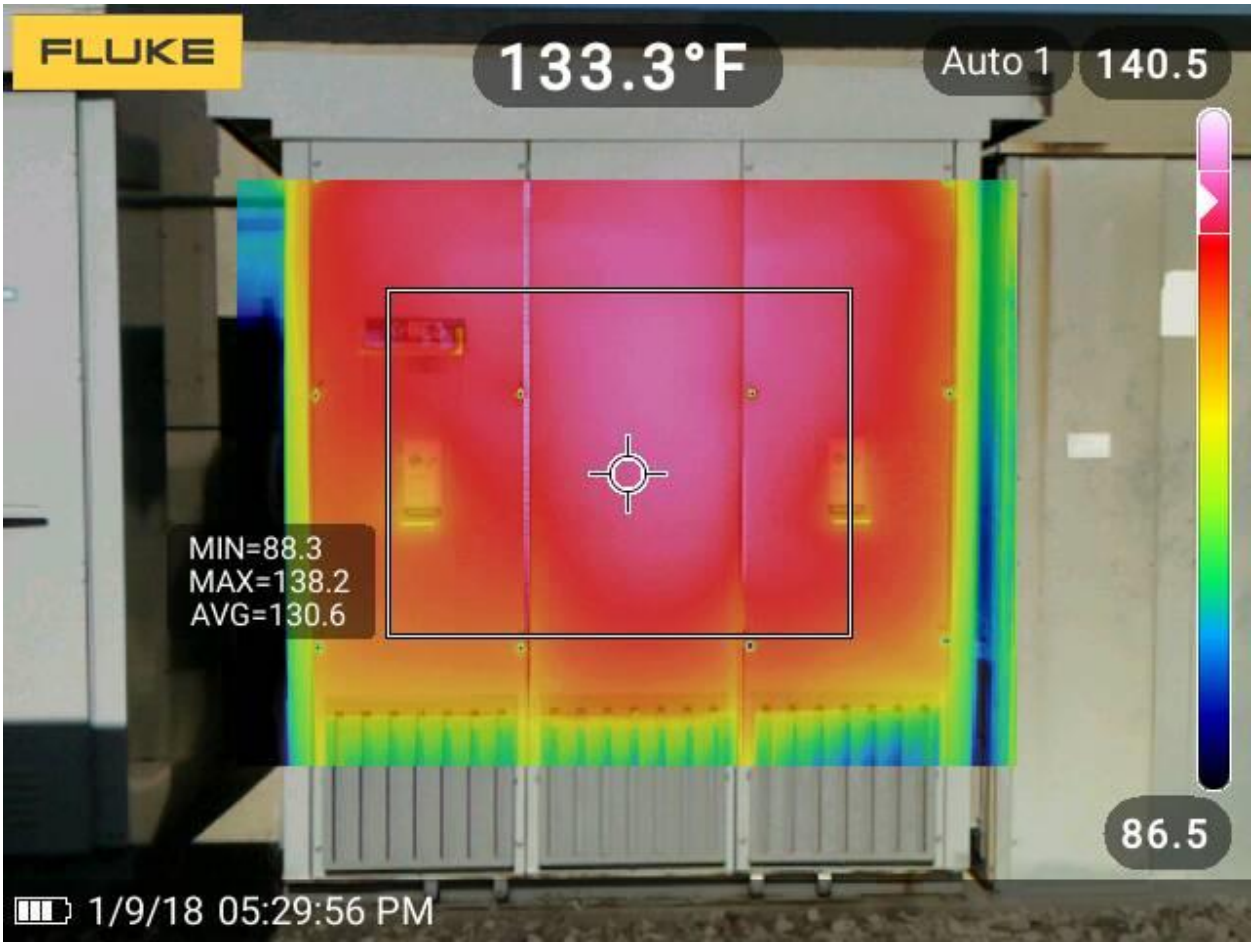

Figure 5-10 Transformer outer cabinet at 20 Hz, this temperature rise was 30F from 15 Hz thermal images.

5.4.2. Bus Bars Temperatures

At 20 Hz the FBS output current was 1695A_{RMS} opposed to 1354A_{RMS} for 15 Hz, an increase of 341A_{RMS}. This variation corresponds with a 56% increase in ohmic power dissipation. The bus bars on the original 16 stations are about 25ft long, the bus runs from the gallery through a penetration which is filled with polyethylene beads for radiation shielding.

Before running the stations at 20 Hz for a prolonged period, a 15 Hz 3-day test was conducted. The temperature rise from 8 hours to 66 hours was 17.5C and was still rising.

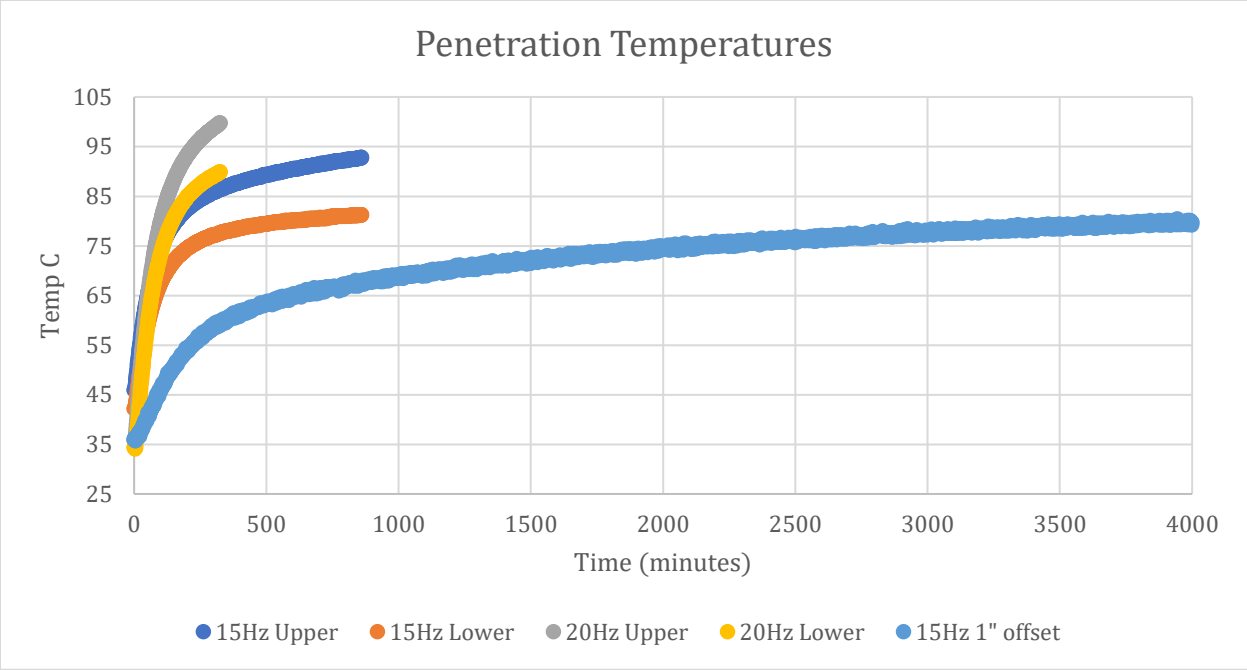

Figure 5-11 Original 3-day 15 Hz run, with second set of tests overlayed

The thermistor was placed as close as possible to the copper bus bar by driving the detector into the polyethylene beads with a long retractable rod. The thermistor was about 1 foot deep into the polyethylene beads, about 11'8" from the top of the penetration. After 8 hours of running at 20 Hz, the polyethylene beads were vacuumed out to verify they hadn't melted. Inspection of vacuumed penetration showed that the thermistor had been off the bus bar by about an inch.

Two thermistors were added to the penetration while there were no polyethylene beads in the penetration, so the exact thermistor locations were known. One was added directly on top of the bus bar at 16' from the top of the penetration (lower) the other was directly on the bus bar at 11'8" from the top of the penetration (upper).

The 15 Hz and 20 Hz measurements were repeated with the new thermometry for an 8-hour test. At 20 Hz, the temperature reached 100C within the first 6 hours operating at 20 Hz and was still significantly increasing. Due to an unknown thermal gradient inside the penetration, the test was

stopped at 100C. Forecasting the trend from the original 15 Hz data test, the penetration temperature would exceed 120C.

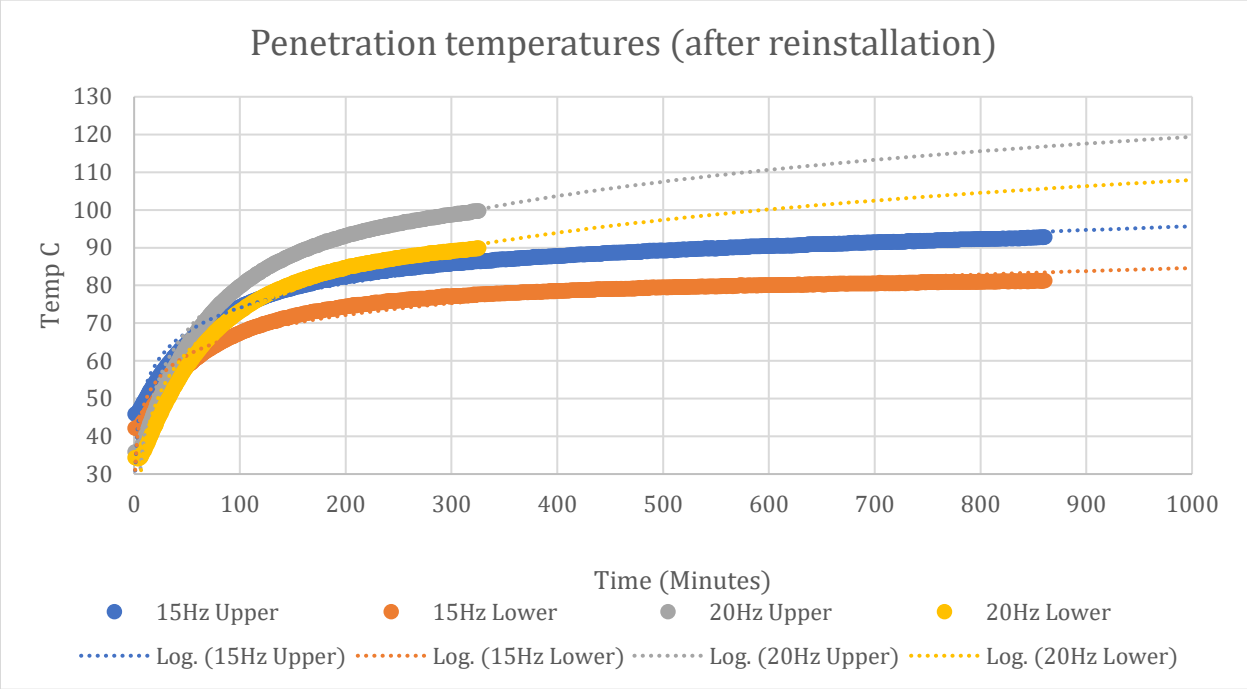

Figure 5-12 Comparison of thermistor readbacks of 8-hour tests.

IR thermal imaging of all the gallery bus bars was also conducted at 15 Hz and 20 Hz. The bus bars are wrapped in Kapton tape, and the emissivity of Kapton was not calibrated for. The air flow through different sections is also variable, which makes station comparisons quite different. Thermal imaging was useful for comparative measurements of the same station but is not an exact measurement.

Figure 5-13 Thermal image of the bus bar from the view of the tunnel

5.5. Tunnel Comparison to Test Cave Data

The data collected from the qualification tests is useful for benchmarking the relative heating of the cavity in the 20 Hz operation. Stations 12 and 22 had recently been tested on the test stand at 15 Hz and were used for a reference set of data. In the stand, the internal contact thermometry temperatures can be taken more quickly, thus showing slightly higher temperatures.

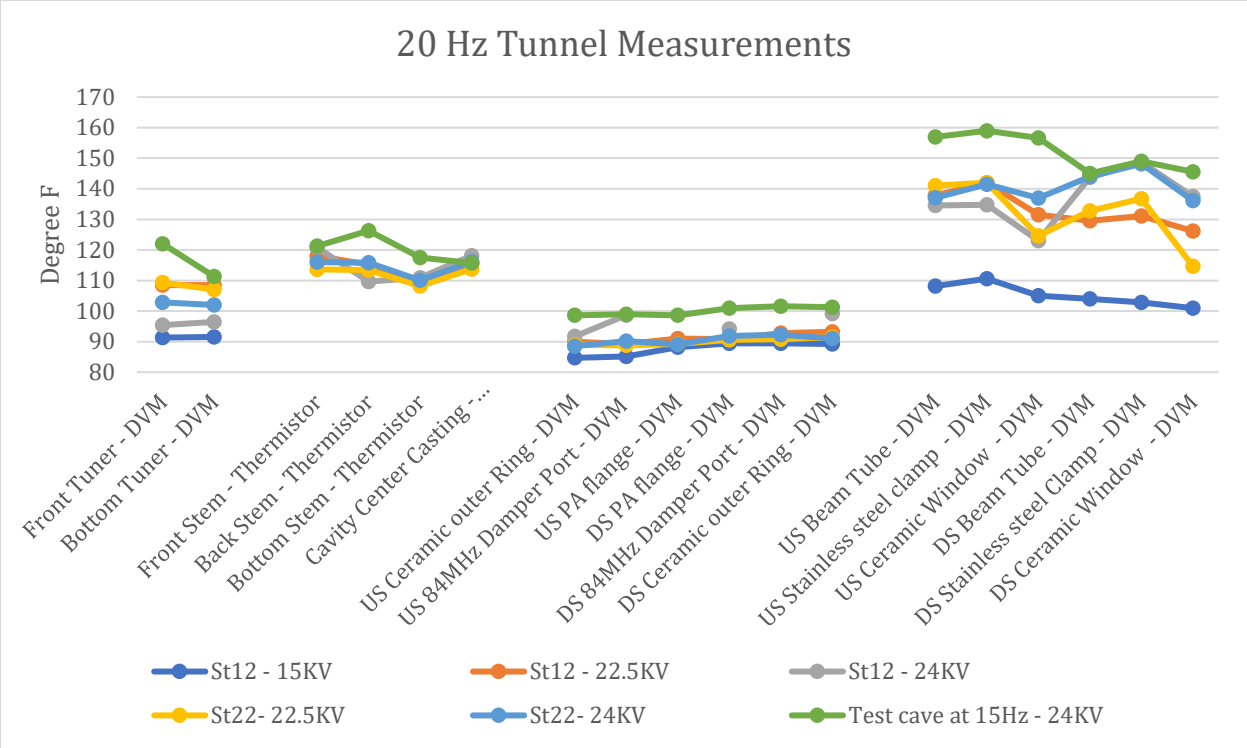

Figure 5-14 Overall comparison of temperatures at various modulator voltages

Table 5-3 Comparison of cavity measured temperatures. The thermistor measurements were taken before turning off. The DVM thermometer measurements were conducted on a tunnel access.

	St12 - 24KV	St22- 24KV	Test cave at 15 Hz - 24KV	
Front Tuner - DVM	95.4	102.8	122	°F
Bottom Tuner - DVM	96.5	102	111.3	°F
Front Stem - Thermistor	32.0	32.0	32.0	°F
Back Stem - Thermistor	32.0	32.0	32.0	°F
Bottom Stem - Thermistor	32.0	32.0	32.0	°F
Cavity Center Casting - Thermistor	32.0	32.0	32.0	°F
US Ceramic outer Ring - DVM	91.7	88.5	98.6	°F
US 84 MHz Damper Port - DVM	98.7	90.2	99	°F
US PA flange - DVM	-	89.1	98.6	°F
DS PA flange - DVM	94.1	91.8	101	°F
DS 84 MHz Damper Port - DVM	-	92.3	101.6	°F
DS Ceramic outer Ring - DVM	99.2	91	101.3	°F
US Beam Tube - DVM	134.6	137.1	157	°F

US Stainless steel clamp - DVM	134.8	141.5	159	°F
US Ceramic Window - DVM	123	137	156.6	°F
DS Beam Tube - DVM	143.8	144	145	°F
DS Stainless steel Clamp - DVM	148.7	148.2	149	°F
DS Ceramic Window - DVM	137.5	136.1	145.6	°F

6. Results Summary and Proposed Changes

The Booster cavity was capable of producing the required RF. Heat load internal and external to the cavity behave comparably to 15 Hz operation. The ceramic windows and associated mounting hardware were within acceptable levels. No sparks were detected during this test. It would be advantageous to run a cavity for 2 or more months in the MI60 test stand for the purpose of reliability testing the bias supply, modulator, and cavity.

The infrastructure specifically pertaining to the bias power supplies highlighted power consumption and unsustainable temperatures. The 15%, 160KVA, increase in apparent power will put the system over the edge of its rated limit. The output of the bias supplies increased by 25%, 341A_{RMS}, this resulted in high temperatures in the bus bars penetration. The data indicates that the polyethylene beads would melt, and the lack of air flow in the region exacerbates thermal stability.

The bias supply was capable of tuning to the new 20 Hz bias program. However, the supply was operating on the edge of its regulation. The new operating program has a higher negative slew rate, therefore further testing is recommended to verify long term functionality.

6.1. Proposed Changes - Tuner Reconfiguration

The original cavities were designed to sweep frequencies of 30-53 MHz. In the PIP-II era the cavities only need to sweep from 44-53 MHz. The frequency program in figure 4-2 highlights the change in requirements for the Booster. The intrinsic frequency of the cavities is 26 MHz, therefore raising the intrinsic frequency to 30 to 34 MHz could allow for a lower total current draw in both galleries. One method of doing this would be to change the ferrite arrangement of the tuners.

During the PIP project, the prototype 3.25” aperture cavity was built, and initially required the bias supply to provide 3000 Amps to reach 52.8 MHz. This was unacceptable, so 4 ferrites from each tuner

were removed, and 4 aluminum blanks were installed. After the change, the bias supply only needed to provide 1850 Amps to reach 52.8 MHz, and the cavities intrinsic frequency increased about 3 MHz.

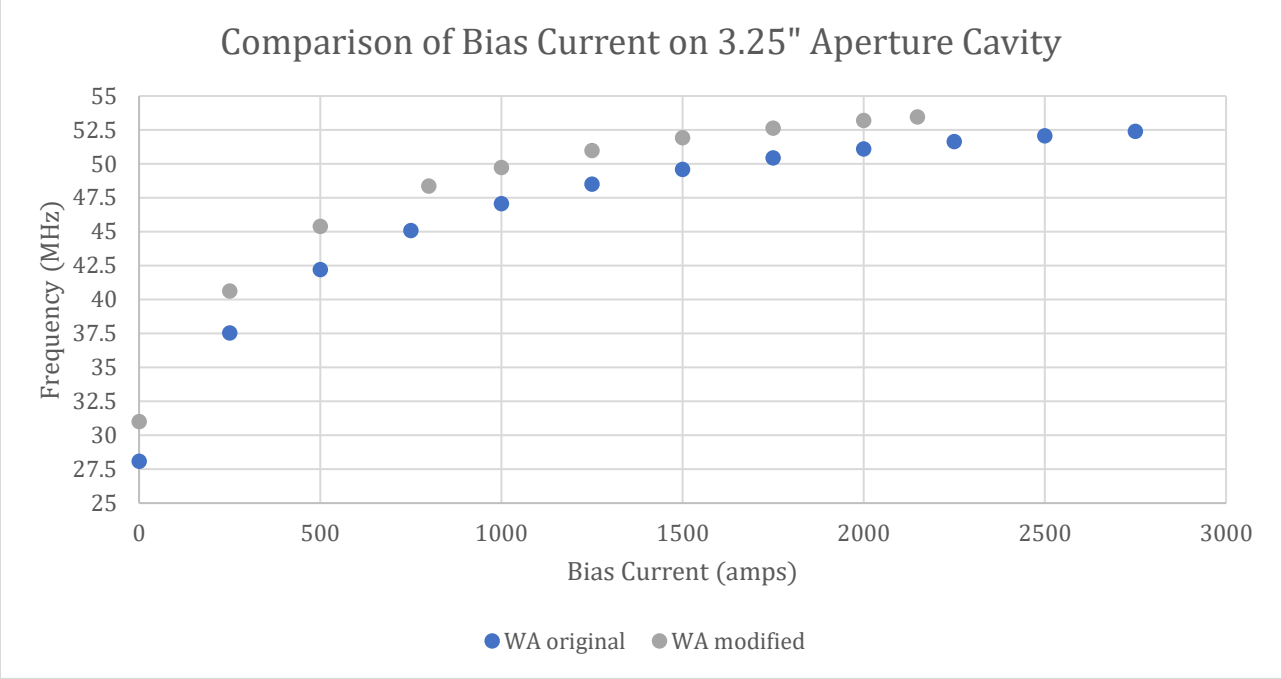

Figure 6-1 Measured frequency of 3.25" aperture cavity before and after tuner manipulations

New simulations of the Booster RF cavities would need to be conducted followed by prototyping the new or modified tuners and testing at full operating gradient on a cavity. If a tuner reconfiguration is pursued, it may also be beneficial to reduce the total number of tuners from 3 to 2. A CST simulation of the cavity model with 2 tuners shows the intrinsic frequency decreases, however, the cavity will be less loaded, and may still have an acceptable dynamic tuning range.

When the tuners are not heavily biased, they have the ability to spark due to a parallel resonance with the cavity. Given the heavily biased nature of the current operation, this is not an issue, but if the tuners were reconfigured, this would need to be analyzed. [14]

6.2. Proposed Change - New Bias Supply

An alternate solution to reduce both the power consumption and the temperature of the bus bar would be to develop new bias supplies with a faster negative slew rate. The RMS current of the ramp down is $1360A_{RMS}$ increasing the negative slew rate would decrease this value. Depending on the power supply topology, it would also be beneficial to have a better power factor than 0.27, preferably with active power factor correction. A new power supply should be designed to fit the needs of both Booster and Main Injector.

6.3. Proposed Change - Bus Bar Modifications

If the proposed changes mentioned above are not pursued, there are alternate options for reducing the temperature of the bus bars. A water-cooling system could be utilized to cool the bus bar, or the bus bar could be replaced with a new bus with larger cross-sectional area. The power loss in the bus bar is due to ohmic losses, and the resistance R is inversely correlated to the cross-sectional area of the conductor.

$$R = \frac{\rho L}{A} \tag{20}$$

If length, L, and resistivity, ρ, of the new bus bar are the same, then using 5x3/8" bus bar to replace the 4x1/4" would decrease by the resistance by 1.875 times. Both water cooling and larger bus bars addresses the symptom of the new operating regime, and not the source of the problem.

7. Conclusions

In the PIP-II era, the operational requirements of the Booster accelerator change significantly. The injection energy will increase from 400 MeV to 800 MeV and the cycle frequency will increase from 15 Hz to 20 Hz. These changes result in a change of the frequency programs, the voltage programs, and other aspects of operations. The work documented in this thesis investigated the impacts to the thermal and power loads on the RF cavities and the support infrastructure.

The RF cavities were found to reliably produce the necessary RF gradient with realistic operating programs. The temperatures inside the cavity at critical mechanical junctions were measured and found to be consistent with current operating temperatures. However, the support infrastructure was found to be inadequately sized for the increase in thermal and power loads. The Booster cavities use biased ferrite tuners, which require higher bias current at higher frequencies. Due to the new frequency program the required RMS current for the tuner bias increased by approximately 25% compared to the present operation see Figure 4-8. This increased the power dissipated on the tuner bus infrastructure and resulted in an unacceptable increase is bus bar temperatures shown in Figure 5-12. The power demand on ferrite bias supplies also increased past what can be provided by the existing 1200KVA transformer infrastructure shown in table 5-2.

Proposed solutions were presented, with different approaches. The first approach is to replace the problematic areas - a new larger bus bar for the bias tuner and higher power transformers for the infrastructure while keeping the cavities the same. The second approach is to modify the tuner design to match the new requirements, which would lower the RMS current requirement to the bias tuner compared to current operation. Such an approach solves the bus bar temperature problems and decreases the power demand on the existing infrastructure.

In conclusion, a successful test of the PIP-II era operating parameters (800 MeV and 20 Hz) was conducted. Several issues were identified, and solutions have been proposed. The PIP-II era

approaches, and the Booster RF systems can adjust and operate so that the Booster accelerator will remain the heartbeat of the lab.

8. Bibliography

[1] J. E Griffin "TM-1519 RF Cavity Primer for Cyclic Proton Accelerators" Available: https://lss.fnal.gov/lists/fermilab-reports-tm.html 1988

[2] J. E Griffin "TM-1968 Aspects of Operation of the Fermilab Booster RF System at Very High Intensity" Available: https://lss.fnal.gov/lists/fermilab-reports-tm.html 1996

[3] W. Merz "Fermilab Operation Bulletin No. 813" 1980

[4] S. Ohnuma "TM-1381 The Beam and The Bucket" Available: https://lss.fnal.gov/lists/fermilab-reports-tm.html 1986

[5] Charles M. Ankerbrandt "FN-650 Design Concepts for a Novel Fermilab Superbooster" Available: https://lss.fnal.gov/lists/fermilab-reports-fn.html 1996

[6] Wiedemann, H. "Particle Accelerator Physics." Springer, Berlin, Heidelberg. https://doi.org/10.1007/978-3-540-49045-6_16 2007

[7] B. Worthel, J. Crawford, W. Pellico, J. Morgan, C. Gattuso, J. Reyna, B. Drendel, T. Sullivan, and C. Broy, "Booster Rookie Book." Available: https://operations.fnal.gov/rookie_books/Booster_V4.1.pdf 2009

[8] Lebedev, V. et al. "The PIP-II Conceptual Design Report." Fermilab Design Report. Available: https://pip2.fnal.gov/_assets/docs/Pip2CD-3_2013-004.pdf 2013

[9] Tan, C.Y. et al. "The 750keV Injector Upgrade Plan." Fermilab AD Document Database, AD-Document-003646, 2017. Available: https://beamdocs.fnal.gov/AD/DocDB/0036/003646/002/project_v1.pdf

[10] "Fermilab Linac Upgrade Conceptual Design: Revision 3". Web. doi:10.2172/1423261. 1989

[11] Q. A Kerns "FN-07 Main Ring RF Notes" Available: https://lss.fnal.gov/lists/fermilab-reports-fn.html 1967

[12] E.D. Courant "FN-187 Longitudinal Space Charge Effects at Transition in the NAL Booster and Main Ring" Available: https://lss.fnal.gov/lists/fermilab-reports-fn.html 1969

[13] W.W. Lee "TM-333 Effects of Nonlinearities on the phase Motion in the NAL Booster" Available: https://lss.fnal.gov/lists/fermilab-reports-tm.html 1971

[14] Berenc, T. and Reid, J. "Main Injector HLRF Anode Limit Program & Cavity Tuner RF Voltage Limit." FNAL Beams Doc 2317 v3. Available: https://beamsdoc.fnal.gov/ops/docs/HLRF/MIRF/anode_limit_program_v3.pdf. 2006

[15] D. Boussard "Design of A Ring RF System" 1991

[16] D. Barak, B. Harrison, and A. Watts, “Concepts Rookie Book.” Available: https://operations.fnal.gov/rookie_books/concepts.pdf 2000

[17] "Calculators for Fluid Heaters." WK Fluid Handling, February 2020, https://wkfluidhandling.com/resources/calculators/.

[18] V. Grzelak et al “Booster RF Book” Available: https://docs.google.com/document/d/1e_TGlmUdvezNjmFe79n6iuC70CPCg5V1rfYWxih3sp0/edit#heading=h.ddhhjpke2ez , February 2020

[19] J. Katz Q Kerns B Sandberg, “Digital Measurement of Ferrite Hysteresis Loops” https://accelconf.web.cern.ch/p69/PDF/PAC1969_0546.PDF 1969

[20] Kerns, Q., Tool, G., & Katz, J. “Ferrite Measurements for synchrotron RF Accelerating System Design” Lawrence Berkeley National Laboratory. LBNL Report #: UCRL-11801. https://escholarship.org/uc/item/3x16k03x 1965

[21] Q.A. Kerns “Ferrite Damping the Main Accelerator Cavities https://inspirehep.net/files/e854181dfd5a9c242899f7cdb6bcda5a 1970

[22] E.L. Hubbard “TM 405 – Booster Synchrotron” Fermilab https://lss.fnal.gov/lists/fermilab-reports-tm.html 1973

[23] Conversations with C.Y Tan

[24] W. R. Smythe, "Reducing Ferrite Tuner Power Loss by Bias Field Rotation," in IEEE Transactions on Nuclear Science, vol. 30, no. 4, pp. 2173-2175, Aug. 1983, doi: 10.1109/TNS.1983.4332751.

[25] Q.A Kerns “The RF Ferrite Testing Program at NAL” 1971

[26] J. Griffin and G. Nicholls “TM655- Notes on “High Loss Effect” in RF Cavity Tuning Ferrite” Available: https://lss.fnal.gov/lists/fermilab-reports-tm.html 1976

[27] J. Dinkel Q.A Kern, L.A Klaisner and G.S Tool “NAL Booster and Storage Ring RF Systems” Available: https://accelconf.web.cern.ch/p69/PDF/PAC1969_0510.PDF 1969

[28] T. Berenc, J. Reid “A Solid-State Driven Power Amplifier Design for the Booster RF Cavities” Available: https://rf.fnal.gov/global/technotes/TN/TN023.pdf 2001

[29] Lee, S. (2018). Accelerator Physics (4th ed.). World Scientific Publishing Company. Retrieved from https://www.perlego.com/book/979029/accelerator-physics-pdf 2018